# Springtime high surface ozone events over the western United States: Quantifying the role of stratospheric intrusions

Meiyun Lin[1,2*], Arlene M. Fiore[2,3], Owen R. Cooper[4,5], Larry W. Horowitz[2], Andrew O. Langford[5], Hiram Levy II[2], Bryan J. Johnson[5], Vaishali Naik[2,6], Samuel J. Oltmans[4], Christoph J. Senff[4,5]

[1]*Atmospheric and Oceanic Sciences, Princeton University, Princeton, New Jersey, USA*
[2]*NOAA Geophysical Fluid Dynamics Laboratory, Princeton, New Jersey, USA*
[3]*now at Department of Earth and Environmental Sciences and Lamont-Doherty Earth-Observatory, Columbia University, Palisades, New York*
[4]*Cooperative Institute for Research in Environmental Sciences, University of Colorado, Boulder, Colorado, USA*
[5]*NOAA Earth System Research Laboratory, Boulder, Colorado, USA*
[6]*UCAR/NOAA Geophysical Fluid Dynamics Laboratory, Princeton, New Jersey, USA*

***Corresponding Author:**
Meiyun Lin
*meiyunl@princeton.edu*
609 452-6551

Draft: May 21, 2012
Submitted to JGR-Atmosphere, CalNex Special Section

**Key Points:**
(1) Stratospheric intrusions can episodically contribute 50-60% to surface ozone
(2) Stratospheric impacts may confound efforts to attain ozone air quality standards
(3) Global high-res model, satellite and *in situ* observations yield process insights

## Abstract

The published literature debates the extent to which naturally occurring stratospheric ozone intrusions reach the surface and compromise attainment of the U.S. National Ambient Air Quality Standard (NAAQS) for ground-level ozone (currently 75 ppbv). Analysis of ozonesondes, lidar, and surface measurements over the western U.S. from April to June 2010 show that a global high-resolution (~50x50 km$^2$) chemistry-

climate model (GFDL AM3) captures the observed layered features and sharp ozone gradients of deep stratospheric intrusions, representing a major improvement over previous chemical transport models. Thirteen intrusions enhanced daily maximum 8-hour average (MDA8) ozone to 60-85 ppbv at surface sites. With a stratospheric ozone tracer defined relative to a dynamically-varying tropopause, we find that transport of stratospheric ozone to the surface can contribute 30-55 ppbv, composing 50-60% of the total, on days when observed MDA8 ozone exceeds the NAAQS. Several of such events occurred in suburban areas of California and Colorado. These stratospheric intrusions elevated background ozone concentrations (estimated by turning off North American anthropogenic emissions in the model) to MDA8 values of 60-75 ppbv. At high-elevation western U.S. sites, the $25^{th}$-$75^{th}$ percentile of the stratospheric contribution is 15-25 ppbv when observed MDA8 ozone is 60-70 ppbv, and increases to ~17-40 ppbv for the 70-85 ppbv range. These estimates, up to 2-3 times greater than previously reported, indicate a major role for stratospheric intrusions in driving springtime high-$O_3$ events, which poses a challenge for attaining the ozone NAAQS, particularly if a threshold in the 60-70 ppbv range were to be adopted.

## 1. Introduction

Understanding global sources of local air pollution is crucial for setting air quality standards and for designing appropriate control policies [*National Research Council, 2009; McDonald-Buller et al., 2011*]. In contrast to the "good" ozone ($O_3$) layer in the stratosphere that shields life on Earth from the Sun's harmful ultraviolet radiation, exposure to high concentrations of ground-level (i.e. “bad”) $O_3$ aggravates respiratory illness [*World Health Organization, 2005*]. Stratosphere-to-troposphere transport (STT) is a common occurrence at mid- and high latitudes, but its influence on tropospheric $O_3$ levels remains a long-standing question despite decades of

64 research [*Levy et al., 1985; Roelofs and Lelieveld, 1997; Monks, 2000; Stohl et al.,*
65 *2003; Stevenson et al., 2006; Wild et al., 2007; Hsu and Prather, 2009*]. In particular,
66 prior publications debate the extent to which stratospheric $O_3$ intrusions reach the
67 surface and compromise attainment of the air quality standard for ground-level $O_3$
68 [*Lefohn et al., 2001, 2011; Fiore et al., 2003; Langford et al., 2009*]. This poor
69 understanding reflects our inability to directly measure the stratospheric contribution
70 to tropospheric $O_3$, as well as limited model capability to represent the dynamic
71 processes of STT and to account accurately for stratospheric $O_3$ in the troposphere
72 [*e.g. Roelofs et al., 2003; Hudman et al., 2004; Hsu et al., 2005; Hess and*
73 *Lamarque, 2007; Zhang et al., 2011*]. Here we revisit the role of stratospheric
74 influence on springtime high surface $O_3$ episodes over the western United States by
75 applying a newly developed global model with fully coupled stratosphere-
76 troposphere chemistry at ~50x50 $km^2$ resolution (GFDL AM3) [*Lin et al., 2012*],
77 which we analyze alongside a suite of satellite and *in situ* measurements.
78
79 The primary mechanism for the transport of stratospheric $O_3$ to the mid- and lower
80 troposphere is descent through the dry airstream of mid-latitude cyclones [*Danielsen*
81 *1968; Johnson and Viezee, 1981; Cooper et al. 2001; Stohl et al. 2003*]. Western
82 North America, located at the end of the North Pacific wave train of mid-latitude
83 cyclones, has been identified as a preferred region for deep STT reaching below the
84 700 hPa level [*Sprenger and Wernli, 2003; James et al., 2003*]. The semi-permanent
85 surface anticyclone in the eastern North Pacific Ocean provides a baroclinic zone
86 that facilitates descent of stratospheric $O_3$ into the lower troposphere following strong
87 frontal passages [*Bourqui and Trepanier 2010*]. The impacts of STT on tropospheric
88 $O_3$ are greatest at extratropical latitudes in winter and spring, when the lifetime of $O_3$
89 is much longer compared to the tropics and to summer, when photochemical and
90 depositional $O_3$ losses maximize [e.g. *Holton et al., 1995*].

Signatures of stratospheric intrusions in the free troposphere have been observed in various contexts. For example, they appear as filamentary dry features in satellite water vapor imagery [e.g. *Appenzeller and Davies, 1992; Wimmers et al., 2003; Felker et al. 2011*] and as layered structures in $O_3$ profiles [e.g. *Roelofs et al., 2003; Thompson et al., 2007*]. They are evident in ozone lidar measurements [e.g. *Browell et al., 1987*; *Langford et al., 1996; Stohl and Trickl, 1999*] and have long been detected by *in situ* aircraft measurements [*Danielsen 1968; Shapiro 1980; Cooper et al., 2004, 2005*].

Despite observational evidence for the presence of stratospheric intrusions in the free troposphere, accurately quantifying the stratospheric contribution to tropospheric $O_3$ in space and time is complicated by the interplay of processes influencing $O_3$ from STT (e.g. circulation and abundances of $O_3$ in the lower stratosphere; an ever shifting, folding tropopause; filamentary intrusions; evolution in transit due to chemical and depositional losses, and dilution). Many global and regional tropospheric chemical transport models (CTMs) do not reproduce well the layered features of stratospheric intrusions measured by ozonesondes and lidar [e.g. *Roelofs et al., 2003; Hudman et al., 2004; Liang et al., 2007; Tarasick et al., 2007*]. Diagnosing the impacts of STT in surface air is further complicated by the coupling between the free troposphere and the boundary layer and by the dominance of local emissions in contributing to high-$O_3$ pollution in urban areas.

The current guidelines from the U.S. Environmental Protection Agency (EPA) state that air quality monitoring data influenced by an extreme stratospheric $O_3$ intrusion may be excluded from regulatory determinations related to violations of the National Ambient Air Quality Standard (NAAQS) for ground-level $O_3$, since these naturally

occurring “exceptional events” are not reasonably controllable by state agencies [*U.S. EPA*, 2007]. The U.S. EPA Region 8 (Figure 1) is particularly susceptible to these events. The identification of such events is challenging, however, given the episodic, transient and localized nature of deep STT and the limited spatial and temporal extent of measurements available to diagnose their presence. The U.S. EPA has relied heavily on the GEOS-Chem global CTM for estimating background $O_3$ for policy assessments [e.g. *Fiore et al., 2002, 2003;* U.S. *EPA 2006; Zhang et al., 2011*], however, studies have shown that GEOS-Chem underestimates the contribution from deep STT events to lower tropospheric $O_3$ [*Hudman et al., 2004*] and is unable to capture observed $O_3$ above 70 ppbv at remote mountain sites in spring [*Emery et al., 2011; Zhang et al., 2011*], which may reflect stratospheric influence.

For the first time, we apply a global high-resolution (~50x50 $km^2$) chemistry-climate model [*Lin et al., 2012*], with a stratospheric $O_3$ tracer defined relative to a dynamically varying tropopause tracer recently proposed by *Prather et al.* [2011], to quantify stratospheric impacts on western U.S. surface $O_3$ in space and time. Our focus on the western U.S. leverages the availability of near-daily ozonesonde and lidar measurements during the 2010 NOAA CalNex field campaign in California [*Cooper et al., 2011; Langford et al., 2012*], which allows for an unprecedented opportunity to evaluate GFDL AM3 on a process level, in particular, its representation of the dynamic processes conducive to surface impacts from stratospheric intrusions.

Section 2 briefly describes the measurements, model simulations, and stratospheric $O_3$ tagging methodology. Section 3 presents several case studies of the strongest and deepest STT events in April-June 2010, using both the model and observations to assess stratospheric influence on the NAAQS exceedances. Section 4

145 summarizes the ability of the GFDL AM3 model to represent the relevant processes.
146 We then synthesize mean and maximum stratospheric contributions to $O_3$ levels at
147 more than 1200 surface monitoring sites and discuss associated policy implications
148 (Section 5).
149
150 **2. Measurements and Model**
151 **2.1 Upper Air and Surface Measurements**
152 We use a combination of water vapor images from the NOAA GOES-West
153 geostationary satellite, total column $O_3$ retrieved from the Atmospheric Infrared
154 Sounder (AIRS) onboard the NASA Aqua satellite [*Susskind et al., 2003*], and NCEP
155 Global Forecasting System Final Analysis (FNL) to provide a large-scale view of
156 observed synoptic conditions favorable for stratospheric intrusions. Further, we gain
157 insights into the deep descent of stratospheric $O_3$ from near-daily balloon-borne
158 ozonesondes launched at six sites in California (Figure 1) between May 10 and June
159 19, 2010 [*Cooper et al., 2011*]. Three of the sonde launch sites were located on the
160 California coast from north to south: Trinidad Head (TH), Point Reyes (RY), and
161 Point Sur (PS). One site, Shasta (SH), was located in the Northern Sacramento
162 Valley. There were also two sites in Southern California: San Nicholas Island (SN),
163 ~140 km southwest of Los Angeles, and Joshua Tree (JT), located in the Mojave
164 Desert on the northwest edge of Joshua Tree National Park. For comparison with
165 ozonesonde measurements, we sample AM3 at the locations and times of sonde
166 launches as described by *Lin et al.* [2012]. We also use observed relative humidity
167 (RH) profiles from the radiosondes to identify the dry layers as a qualitative proxy for
168 air of stratospheric origin (note we do not use the RH profiles at SN, which are found
169 to be unreliable).
170
171 The $O_3$ distribution in the lower troposphere was also measured by a downward

looking lidar on the NOAA Twin Otter aircraft during two intrusions (May 23 and 29) over Southern California [*Alvarez et al., 2011; Langford et al., 2012*]. We average the lidar measurements over a 0.5°x0.625° grid for direct comparison to the AM3 results sampled along the flight track.

Finally, we investigate ground-based measurements of $O_3$ from the U.S. EPA's Clean Air Status and Trends Network (CASTNet), with sites mostly located in rural areas, and from the Air Quality System (AQS), with sites predominantly clustered in urban areas, for changes of surface $O_3$ levels following the appearance of enhanced $O_3$ in the free troposphere observed by sondes or lidar. Fifteen high-elevation (>1.4 km above mean sea level, a.s.l.) CASTNet and AQS sites (green symbols in Figure 1) are selected to represent general patterns of stratospheric influence in the mountainous regions. We focus our analysis on daily maximum 8-hour average $O_3$ (hereafter MDA8 $O_3$), which usually includes the afternoon hours when the boundary layer is sufficiently deep to mix $O_3$ aloft down to the surface.

### 2.2 GFDL AM3 Model Simulations

AM3 is the atmospheric component of the GFDL global coupled atmosphere-ocean-land-sea ice model (CM3) [*Donner et al*., 2011]. We have recently applied a new version of AM3 at C180 cubed-sphere grid horizontal resolution (~42-63 km) to study transport of Asian $O_3$ pollution to the western U.S. surface [*Lin et al., 2012*]. Model simulations at the C48 resolution (163-231 km) starting in January 2009 were used to initialize the C180 (~43-62 km) simulations spanning January-June 2010. The C180 model outputs are then regridded to 0.5°x0.625° latitude-longitude grid for analysis. To enable direct comparisons with CalNex observations, horizontal winds in our AM3 simulations are nudged to those from the NCEP GFS (approximately 1.4°x1.4°, 64 sigma levels, archived 3 hourly), utilizing a weaker nudging strength with decreasing pressure as described by *Lin et al* [2012] (i.e., relaxing with a time

scale of 6 hours in the surface level and ~60 hours at 100 hPa to minimize the impacts of noise near the tropopause introduced via nudging).

Major AM3 model updates since *Lin et al* [2012] include: (1) implementing the Fast-JX photolysis scheme [*Wild et al, 2000*] coupled to cloud and aerosol properties in the AM3 radiation scheme [*J. Liu, personal communication, 2011*], and (2) using global anthropogenic emissions from RCP8.5 for 2010 [*Moss et al., 2010*] to better represent recent emission changes in Asia, North America, and Europe. We find that $NO_x$ emissions in RCP8.5 for 2010 are approximately 35% lower over heavily populated regions than that in the U.S. National Emission Inventory (NEI) for 2005, consistent with changes in the 2005–2010 satellite measurements of $NO_2$ columns from the SCIAMACHY sensor (data available on *www.tenis.nl*).

Accurate representation of $O_3$ levels in a stratospheric intrusion depends strongly on $O_3$ simulated in the lower stratosphere [*Roelofs et al., 2003*; *Terao et al., 2008*]. AM3 includes fully coupled stratosphere-troposphere-aerosol chemistry within a general circulation model [*Donner et al., 2011*], with 48 vertical levels, ranging in thickness from 70 m near the Earth's surface to 1-1.5 km near the tropopause and 2-3 km in much of the stratosphere. This full-chemistry feature, described more fully in Naik et al., in prep, distinguishes the GFDL AM3 model from most current generation global tropospheric CTMs, which represent stratospheric $O_3$ distributions with simplified stratospheric chemistry (SYNOZ or LINOZ) or by relaxing to an observed climatology [*McLinden et al., 2000; Horowitz et al., 2003; Fiore et al., 2003; Emmons et al., 2010; Zhang et al., 2011*], and enables a process-oriented analysis of stratospheric interactions with tropospheric chemistry. Observed sea surface temperatures and sea ice, well mixed greenhouse gas and halogen concentrations, and optical properties of stratospheric aerosols are specified in AM3 as time-varying

fields. The major stratospheric $O_3$ destruction cycles ($O_x$, $HO_x$, $NO_x$, $ClO_x$, and $BrO_x$) are included explicitly in the model, as well as heterogeneous reactions on ice and nitric acid trihydrate (NAT) in polar stratospheric clouds (PSCs) *[Austin and Wilson, 2006; 2010*].

In addition to the standard simulation, we conducted a sensitivity simulation with North American (NA) anthropogenic emissions switched off in the model to estimate background $O_3$ levels, defined by U.S. EPA as $O_3$ concentrations that would exist in the absence of anthropogenic emissions from U.S., Canada, and Mexico (previously referred as policy relevant background $O_3$ [*McDonald-Buller et al*., 2011]; hereafter NA background). The specific sources of the NA background include STT, intercontinental transport (e.g. Asian pollution), and ozone produced by wildfire effluents, biogenic emissions, methane, and lightning $NO_x$. In Section 5, we compare our estimates of the stratospheric component (Section 2.3) of NA background with the Asian pollution estimates as described by *Lin et al.* [2012].

### 2.3 Quantifying Stratospheric Contributions to Troposphere Ozone

We implement the e90 tracer proposed by *Prather et al* [2011] to more accurately diagnose the three-dimensional tropopause location as required to tag $O_3$ originating from the stratosphere ($O_3S$). It should be noted that the AM3 simulation of ozone from STT is entirely driven by winds, with no dependency on the definition of tropopause. The e90 tropopause tracer is applied only for the $O_3S$ tagging as described below.

With a globally uniform surface source and 90-day e-folding lifetime, the e90-tropopause tracer differentiates tropospheric air by time scales, linking it to the mixing of the troposphere and its exchange with the surface. The e90 tracer approach allows for clear characterization of stratospheric vs. tropospheric air in

**253** complex situations where the traditional tropopause definitions (e.g. thermal lapse
**254** rate, potential vorticity, or $O_3$) are problematic. The tropopause value of e90 is
**255** derived as 85 ppbv in the GFDL AM3 model from the constraint that the troposphere
**256** annually comprises about 80% of the atmosphere [*Prather et al, 2001; 2011*].
**257** Monthly mean e90-tropopause pressures and $O_3$ concentrations in AM3 reproduce
**258** the salient features of a climatology derived from ozonesondes (not shown). The
**259** global net stratosphere-to-troposphere flux of $O_3$, diagnosed as the net change due
**260** to advection in each grid cell up to the e90 tropopause archived from the model
**261** every 3 hours, is ~535 Tg/yr in the GFDL AM3 model, within the observation-based
**262** range of 400-600 Tg/yr [*e.g. McLinden et al., 2000; Hsu et al., 2005*].
**263**
**264** We set the $O_3S$ tracer equal to simulated $O_3$ in stratospheric air (e90 < 85 ppbv) and
**265** subject it to chemical loss in tropospheric air (e90 >= 85 ppbv) and depositional loss
**266** to the surface in the same manner as $O_3$ of tropospheric origin. Aged tropospheric
**267** air occasionally includes e90<90 ppbv below 600 hPa in the tropics [*Prather et al.,*
**268** *2011 and M. Prather, personal communication, 2011*], so we restrict tagging $O_3S$ to
**269** above 600 hPa. Ozone in the stratosphere has been spun up for decades. The $O_3S$
**270** and e90 tracers have been spun up for three years in a previous simulation.
**271** Transport of $O_3$, $O_3S$, and e90 are fully driven by meteorology, with no dependency
**272** on the definition of tropopause.
**273**
**274** This stratospheric $O_3$ tagging methodology has a number of mechanistic and
**275** conceptual advantages over the methods used in prior publications. First, the e90
**276** methodology is less prone to errors associated with defining the tropopause in
**277** complex synoptic conditions (e.g. mid-latitude frontal zones), as compared to using a
**278** tropopause fixed at the 100 hPa level [*Roelofs and Lelieveld, 1997; Lelieveld and*
**279** *Dentener, 2000*] or defined by the 2 K $km^{-1}$ thermal lapse rate [e.g. *Emmons et al.,*

*2003*; *Lamarque and Hess, 2004; Lin et al., 2012*]. In the latter methods, any $O_3$ above the "tropopause" is instantly labeled as "stratospheric" regardless of its true origin. We find that the lapse-rate based tagging method overestimates $O_3S$ in surface air by 5-8 ppbv on seasonal average, and occasionally by ~30 ppbv during individual events when e90 indicates an influence of tropospheric background rather than a stratospheric intrusion (not shown). Second, the $O_3S$-e90 tagging method also avoids potential noise that may bias the $NO_x$ tagging technique in which the stratospheric contribution is determined as the residual between two much larger numbers [*Hess and Lamarque, 2007; Pfister et al., 2008*].

Third, the dynamical coupling of stratospheric chemistry and transport with the troposphere in AM3, as opposed to imposing a climatological STT $O_3$ flux in previous models [e.g. *Fiore et al., 2003; Zhang et al., 2011*], allows AM3 $O_3S$ to better capture the dynamic variability of mid- and upper tropospheric $O_3$ due to stratospheric influence. Finally, the new $O_3S$ tracer, implemented in a full-chemistry model like GFDL AM3, accounts for the impacts due to long-range transport and chemical losses of transported stratospheric $O_3$ in tropospheric air as compared to a tracer in a passive trajectory model like FLEXPART [e.g. *Cooper et al., 2005; Langford et al., 2012*] (Figure S5).

## 3. Contribution of Deep Stratospheric Intrusions to Surface Ozone Episodes

### 3.1 April-June 2010: An Active Period for Deep Intrusions

Spring 2010 was unusually cool along the U.S. West Coast with strong surface cold fronts and amplified upper level troughs. We find an ~30% positive anomaly in total $O_3$ columns retrieved from NASA AIRS [*Susskind et al., 2003*] over the northwest U.S. in May 2010 relative to a climatological mean, consistent with the 39% above average $O_3$ enhancements at 7-10 km above California noted by *Cooper et al* [2011]. According to the NOAA Climate Prediction Center (http://www.cpc.ncep.noaa.gov),

307 the 2009-2010 winter was influenced by strong El Niño conditions. Several studies
308 have suggested enhanced STT in winter and spring over western North America
309 following El Niño conditions [*Langford et al, 1998; Koumoutsaris et al., 2008*].
310
311 Indeed, thirteen stratospheric $O_3$ intrusions occurred in April-June 2010 (Table 1). Six
312 events were measured by *in situ* and remote sensing instruments deployed during
313 the CalNex field campaign from May 9-June 20. *Lin et al.* [2012] identified two cases
314 of these intrusions (May 17-20 and June 16-19) that were mixed with Asian $O_3$
315 pollution. *Langford et al* [2012] used principal component analysis (PCA) of $O_3$
316 measurements together with meteorological parameters to infer that these intrusions
317 can account for ~13% of surface $O_3$ variability in the Los Angeles area during
318 CalNex. Here we further explore five of the strongest intrusions (June 7-8, June 9-14,
319 May 27-29, May 22-24, and April 12-14) in Sections 3.2-3.4 and quantify their
320 impacts on western U.S. surface $O_3$. Section 3.5 summarizes the influence of all
321 thirteen events on the day-to-day variability of surface $O_3$ from April-June 2010.
322
323 **3.2 Dynamic Processes Conducive to Surface Impacts: June 7-14 Intrusions**
324 We examine in this section the dominant meteorological conditions favorable for the
325 direct transport of stratospheric $O_3$ to the surface of the Northwest versus the
326 Southwest U.S., as illustrated by the June 7-14 intrusions.
327
328 Figure 2 depicts the development and intensification of two southeastward
329 penetrating upper-level troughs during June 7-12 and their impacts on the downward
330 transport of stratospheric $O_3$ to the lower troposphere. On June 7, the dry airstream
331 of a mid-latitude cyclone was advected southeastward towards the northwest U.S.
332 (Figure 2a), visible as the dry feature (green and blue) in the water vapor image
333 (Figure 2d). A latitude-height curtain plot of $O_3$ distributions in AM3 reveals that $O_3$

from a tropopause fold descended isentropically toward the south to as low as 1 km above the surface off the coast of Los Angeles (Figure 2g). The June 7 and 8 soundings launched along the California coast recorded approximately 80 ppbv of $O_3$ and lower than 5% of RH at 1.0-3.5 km a.s.l. (Figure 3, 1$^{st}$ row). These features strongly support the existence of a sharp layer of enhanced $O_3$ above the boundary layer, attributed to stratospheric origin by AM3. Ozone enhancements were also detected at the surface monitoring sites in Idaho, Utah and Wyoming on June 8, leading to MDA8 $O_3$ in excess of 70-75 ppbv (Figure 4, top panels). AM3 estimates 20-35 ppbv of stratospheric contribution in these locations, although it slightly displaces the peak levels in surface air to the northwest.

Between June 9 and 10, a new upper-level trough formed and propagated southeastward to Northern Nevada (Figure 2, 2$^{nd}$ column). The June 9-10 soundings over Shasta, located on the western edge of the trough, measured >150 ppbv of $O_3$ within the tropopause fold at 9 km a.s.l., while both the Point Reyes and Point Sur sondes captured stratospheric $O_3$ remnants at 2-6 km a.s.l. (Figure 3, 2$^{nd}$ and 3$^{rd}$ row). By June 10, observed $O_3$ at Joshua Tree increased by a factor of 4 between 4 and 6 km from the previous day, indicating the arrival of stratospheric air to the lower troposphere of Southern California. At the surface downwind of the trough (Figure 4, 2$^{nd}$ row), the Nevada Great Basin and California Mojave Desert experienced elevated $O_3$ with stratospheric $O_3$ contributing as much as ~50% of the total in the model.

By June 12, this intrusion evolved into an elongated (~2000 km) and slender (~200 km) streamer, which is visible in the GOES-West water vapor image (Figure 2f) and represented in AM3 as greater than 4-5 PVU of potential vorticity at 250 hPa (Figure 2c). Isentropic descent of stratospheric $O_3$ detached from the tropopause led to the

formation of a distinct $O_3$ layer between 3 and 5 km above the California coast in the model (Figure 2i), in remarkable agreement with $O_3$ profiles measured by the June 12 soundings at Point Reyes, Point Sur, and Shasta (Figure 3, 4$^{th}$ row). In contrast to the coastal sites, the Joshua Tree sounding located in the vicinity of a cut-off low (Figure 2c) captured enhanced $O_3$ in the tropopause fold at 8 km a.s.l.

Injected stratospheric $O_3$ from this cut-off low was transported into surface air over the Southwest between June 12 and 15 (Figure 4, 3$^{rd}$ and 4$^{th}$ rows). The PCA of Langford et al [2012] shows a corresponding peak in the stratospheric contribution to surface air in the Los Angeles Basin on June 12. Transported stratospheric $O_3$ enhanced MDA8 $O_3$ above 70 ppbv at surface monitoring sites as far south as the U.S. Mexico border on June 14 (not shown). By June 15, six days after the initial tropopause fold over the U.S. West Coast on June 9, widespread entrainment of stratospheric $O_3$ into the boundary layer still contributed 30-40 ppbv to MDA8 $O_3$, and when combined with locally produced $O_3$ led to MDA8 $O_3$ levels in excess of 60 ppbv over the entire Southwest region.

The dynamic processes discussed above indicate an important role of deep stratospheric intrusions in driving the regional variability of surface $O_3$ over the western U.S. (e.g. Figure 4). Stratospheric intrusions that remain close to the polar jet stream above Southern Canada and the Northern U.S. primarily affect the surface of Wyoming, Utah and Colorado located immediately in the southern flank of the polar jet (e.g. June 7-8). In contrast, intrusions that break away from the polar jet as they advect toward the south are more effective at transporting $O_3$ to the lower troposphere of the Southwest and into surface air over regions within California, Arizona and New Mexico (e.g. June 9-14).

### 3.3 Stratospheric Influence on a Polluted Region: The May 27-29 Intrusion

A qualitatively similar meteorological situation occurred on May 27-29 (Figure S4). This intrusion appeared as a filamentary feature extending from the Gulf of Alaska to the California coast on May 27. A strong surface anticyclone developed over the eastern North Pacific Ocean on May 28, facilitating more effective transport of stratospheric $O_3$ to the lower troposphere of Southern California during this intrusion as compared to other events.

The May 28 soundings measured an approximately 2-km thick layer of elevated $O_3$ in excess of 100-150 ppbv sloping from 5-7 km above Northern California (Point Reyes and Shasta) to 2-4 km above Southern California (Joshua Tree and San Nicholas), coincident with decreasing RH, a marker for air of stratospheric origin (Figure 5). The elevated-$O_3$ layer just 2 km above Joshua Tree National Park persisted from May 28 through May 29, when it was also measured by an aircraft-based lidar [*Langford et al., 2012*]. AM3 captures these narrow layers of enhanced $O_3$ and estimates a stratospheric contribution of approximately 75%.

Given that San Nicholas Island and Joshua Tree National Park are each located just ~150 km away from the densely populated Los Angeles Basin, locally produced pollution may impact the lower free troposphere of this region under favorable meteorological conditions. Here we find in the model that simulated $O_3$ changes little at 2-5 km above both sites on May 28-29 after switching off NA anthropogenic emissions (green lines in Figure 5), supporting a dominant source from the stratosphere as inferred from the $O_3S$ tracer.

We next examine transport of this enhanced $O_3$ aloft to the surface over the greater Los Angeles area and further east across the Mountain West. Figure 6 shows that surface $O_3$ mixing ratios at Joshua Tree rapidly increase during the growth of

415 daytime boundary layer on May 28 coincident with a substantial decrease in specific
416 humidity, indicating the influence of subsiding dry air from the free troposphere. A
417 similar phenomenon occurred at the surface monitoring sites in Arizona and
418 Colorado on the following day owing to eastward transport. These measured
419 features support attribution to stratospheric origin based on AM3 $O_3S$ for these
420 observed MDA8 $O_3$ enhancements in surface air (Figure 7). At several sites in
421 Arizona and Colorado where observed MDA8 $O_3$ exceeds the 75 ppbv NAAQS
422 threshold, the model estimates a stratospheric contribution of 50-60%.
423
424 Widespread entrainment of stratospheric $O_3$ into the boundary layer on May 29 led
425 to ~10 ppbv increases in observed MDA8 $O_3$ over the entire Los Angeles Basin from
426 the previous day (not shown). AM3 shows that the stratospheric contribution is 40-
427 50% of total MDA8 $O_3$ in the model (Figure 7), representing the largest impacts over
428 the Los Angeles area during CalNex, consistent with the PCA analysis by *Langford*
429 *et al*. [2012]. The AM3 $O_3S$ tracer over Southern California shows a synoptic
430 deviation of up to 20-30 ppbv from monthly mean (Figure S5), similar to an $O_3S$
431 tracer from the FLEXPART trajectory model using a domain filling technique that
432 does not include stratospheric influence on the background [*Langford et al., 2012*].
433 AM3 estimated a corresponding peak in $O_3S$ mixing ratios on some days (e.g. May
434 20-22, May 28-29, June 10-11) when observed $O_3$ at Joshua Tree increases to 60-
435 80 ppbv, implying that direct transport of stratospheric $O_3$ to the surface can
436 occasionally enhance surface $O_3$ to levels near the NAAQS threshold over Southern
437 California. We note that these $O_3$ enhancements are not as strong as on highly
438 polluted days, which are dominated by local influence from the Los Angeles area
439 (e.g., June 4-5, when the stratospheric influence is weakest).

440 **3.4 Stratospheric Influence over the Four Corners Region: The May 22-24 and**
441 **April 12-14 Intrusions**

442 We next present two cases of stratospheric intrusions primarily affecting surface $O_3$
443 over the Four Corners Region (Utah, Colorado, Arizona, and New Mexico). On the
444 afternoon of May 23, the airborne lidar aboard the NOAA Twin Otter aircraft
445 measured $O_3$ mixing ratios greater than 150 ppbv at ~4.5 km a.s.l. along a flight leg
446 ~10 km south of Joshua Tree (Figure 8). AM3 reproduces this enhanced-$O_3$ layer
447 and attributes a stratospheric contribution in excess of ~100 ppbv, indicating the
448 penetration of an unusually large tropopause fold over Southern California. This
449 tropopause fold was also measured by the ozonesondes on May 21-22 when it was
450 located in the upper troposphere over Northern California (Figures S2-S3).
451
452 While ozonesonde or lidar measurements were not available to confirm the presence
453 of the April 12-14 intrusion in the free troposphere, the AIRS instrument onboard the
454 NASA Aqua satellite captured a large-scale column enhancement of polar
455 stratospheric $O_3$ extending to the U.S. West Coast on the afternoon of April 12
456 (Figure S1).
457
458 Intrusions on both May 22-24 and April 12-14 directly led to elevated surface $O_3$ over
459 the U.S. Mountain West (Figure 9). For both events, the GFDL AM3 model
460 reproduces well the 60-85 ppbv range of observed surface $O_3$ at 25 urban and rural
461 sites and estimates approximately 50-75 ppbv of $O_3$ in the absence of NA
462 anthropogenic emissions (green points). The $O_3S$ tracer (blue points) indicates that
463 ~50-60% of the NA background is of stratospheric origin.
464
465 The April 12-14 intrusion was the strongest intrusion during April-June 2010 affecting
466 the surface areas over Colorado. Thirteen surface monitoring sites in Boulder,
467 Denver and Colorado Springs, including six sites in metropolitan areas, experienced
468 peak MDA8 $O_3$ concentrations greater than or equal to the 75 ppbv NAAQS

threshold during April 12-14 on days when $O_3S$ indicates a stratospheric contribution of 40-55 ppbv (Figure 9d). Figure 10 shows that the surface regions experiencing high stratospheric influence in excess of 40 ppbv on April 13 are where the observed total $O_3$ pattern is enhanced. This intrusion pushed MDA8 $O_3$ concentration to 80-86 ppbv at several sites near Colorado Springs on 13-14 April 2010, comparable to the extreme case on 6 May 1999 described by *Langford et al* [2009].

### 3.5 Overall Stratospheric Impacts on Surface Ozone Variability

Time series of MDA8 $O_3$ from April-June 2010 at high-elevation western U.S. sites reveal thirteen observed episodes of 2-3 day duration where MDA8 $O_3$ > 60 ppbv are associated with increasing $O_3S$ in the model surface layer (Figure 11; Table 1). Despite variations in the surface impacts of individual events, consistent synoptic patterns in AIRS total $O_3$ observations, GOES-West water vapor imagery, and GFS FNL analyses confirm the occurrence of favorable meteorological conditions during all thirteen events for transporting stratospheric $O_3$ to the surface, either directly within a deep intrusion, or from upper tropospheric background air that was enhanced by a recent intrusion.

There is a marked case-to-case variability in the intensity and surface destination once stratospheric $O_3$ detaches from the intrusion. Only a very deep trough that traverses the California coast is likely to influence the southwestern U.S. surface, a phenomenon that was particularly active in the late spring and early summer of 2010 (Section 3.1). Our analysis indicates that stratospheric intrusions are not just limited to surface $O_3$ enhancements over the central western and northern U.S. as noted by several studies [e.g. *Langford et al., 2009; Lefohn et al., 2011*]. Occasionally they can directly lead to episodes of elevated surface $O_3$ as far south as the vicinity of the U.S. southwestern border. For example, the AQS site (~2 km a.s.l.) near Silver City located in Southern New Mexico recorded peak MDA8 $O_3$ of

70-80 ppbv approximately 1-2 days after the passage of upper-level troughs, coincident with rising $O_3S$ mixing ratios in the model (Figure 11, right panel). Two days after the May 11 intrusion measured at the free troposphere of California [*Langford et al., 2012; Neuman et al., 2012*], observed MDA8 $O_3$ exceeds 70 ppbv at Big Bend National Park in Southwestern Texas, representing the southern most surface impacts from stratospheric intrusions during CalNex.

Figure 11 shows that the GFDL AM3 model generally captures observed synoptic variability of MDA8 $O_3$ in surface air, which is dominated by background influence (primarily stratospheric $O_3$ intrusions) rather than by regional pollution. For the day-to-day variability, the correlation coefficients of simulated $O_3$ with observations range from 0.42-0.74 for the total, from 0.32-0.62 for the NA background, and from 0.22-0.66 for the stratospheric contribution. At several sites (e.g. GRB, GRC, CAN), the higher correlation of NA background with observations as compared to $O_3S$ reflects the influence of Asian pollution events (e.g. May 8-9 and June 20-22) [*Lin et al., 2012*].

## 4 Overall GFDL AM3 Evaluations

### 4. 1 Stratospheric Intrusion Processes

On the basis of the process-oriented evaluation in Section 3, we conclude that the GFDL AM3 model with ~50x50 $km^2$ horizontal resolution, nudged to GFS winds, reproduces the principal features of deep stratospheric intrusions, including the evolution of synoptic conditions, the descent of detached stratospheric $O_3$ to the lower troposphere, and its impacts on episodes of elevated $O_3$ in surface air. Specifically, AM3 resolves the filamentary features of stratospheric intrusions observed in the satellite imagery (Figures 2, S1-S4, *Lin et al*., 2012), indicating the nudging technique succeeds in capturing the key synoptic conditions. Analysis of ozonesonde and lidar measurements (Figures 3, 5, and 8) demonstrates that AM3

reproduces the observed layered structure, sharp $O_3$ gradients of deep intrusions and associated day-to-day variability of $O_3$ over the western U.S. mid- and lower troposphere, a marked improvement upon previous models [e.g. *Roelofs et al., 2003; Hudman et al., 2004; Liang et al., 2007*].

The e90-based $O_3S$ tracer tagging technique (Section 2.3) provides a robust method for estimating the contribution of STT to tropospheric $O_3$. For example, the greatest concentrations of $O_3S$-90 tracer in the troposphere typically occur at the altitudes where observed RH suggests influence of dry air from the stratosphere. These intrusion layers also coincide with the enhanced background (green lines in Figures 3 and 5), which is dominated by the stratospheric contribution but estimated independent of the $O_3S$ tagging technique.

AM3 has a tendency to overestimate $O_3$ both in the upper troposphere (e.g. top row of Figure 3) and lower troposphere (e.g. bottom row of Figure 3). It is unclear that these biases can be fully attributed to excessive stratospheric influence as the bias is typically smallest at the altitude with strongest stratospheric influence. At several locations (e.g. at SH on June 9-10 and RY on June 10), the model is clearly overestimating $O_3$, which may reflect too much stratospheric influence. We next examine any relationship between the model surface $O_3$ biases and this potentially excessive stratospheric contribution to the lower free troposphere.

### 4.2 Surface Ozone

The model surface $O_3$ is biased high by ~6 ppbv on average over the intermountain west. During observed high-$O_3$ episodes, there is no evidence for a systematic model bias in surface $O_3$ over the Rocky Mountains in Wyoming and Northern Colorado (Figure 11, 1$^{st}$ column). In contrast, the model consistently overestimates the observed MDA8 values by up to 10-20 ppbv in Arizona and New Mexico, which

seems to reflect excessive stratospheric influence (Figure 11, 3rd column, auxiliary Figure S6). The model typically spreads the $O_3$ enhancement across a wider range of sites over the Southwest rather than capturing the observed localized features (e.g. April 6-7). While the source of this problem is difficult to fully attribute, it may reflect inadequate representation of boundary layer mixing with the free troposphere, combined with limited resolution of sharp topography and meso-scale meteorology. These representation problems likely also contribute to offsets in the timing and placement of peak stratospheric impacts in surface air (e.g. Figure 4).

Figure 12 shows that our estimated stratospheric influence is moderately correlated ($r^2$=0.38-0.46) with model biases across the central western U.S. between 38-45° N (box in Figure 1) and high-altitude sites across the intermountain west when observed MDA8 $O_3$ exceeds 60 ppbv. The correlation does not necessarily indicate a systematic model overestimate of stratospheric contribution to high-$O_3$ events as both under- and over-estimates occur. Indeed, the $r^2$ values decrease to 0.18-0.26 for all points with positive biases.

We next attempt to remove the influence of excessive STT (such as may occur due to problems with resolving the timing and spatial location of deep intrusions, particularly in the SW region) in the lower troposphere and surface air. In places where we have observational constraints, we apply a bias correction to the simulated stratospheric and NA background contributions to surface $O_3$. For each day, at all sites where AM3 overestimates observed MDA8 $O_3$ and where the estimated stratospheric contribution exceeds the model bias, we assume that the bias is caused entirely by excessive stratospheric $O_3$. We thus subtract this bias from the AM3 estimate of stratospheric $O_3$ and NA background. The results thus represent a conservative estimate for stratospheric influence on surface $O_3$ as reported in

577 Section 5 (note that we do not correct for underestimates).

578

579 **5. Statistics of Stratospheric Impacts on U.S. Surface Ozone in Spring**

580 We summarize in this section the overall statistics of stratospheric impacts on
581 springtime ground-level $O_3$ drawing upon more than 10,000 samples of MDA8 $O_3$
582 measurements and model results from April-June 2010, and discuss the implications
583 for attaining the $O_3$ NAAQS in western U.S. urban and rural areas.

584 **5.1 Regional Variability across the Continental U.S.**

585 Figure 13a shows that the western U.S. is the region where STT contributes most
586 surface $O_3$ concentrations in spring, reflecting a combination of more frequent
587 erosion of cut-off lows during strong frontal passages and a higher elevation to
588 intersect stratospheric $O_3$ subsiding behind cold fronts. The minimum stratospheric
589 influence in surface air occurs in the Southeast, where air masses advected from the
590 Gulf of Mexico limit influence from westerly transport in the lower troposphere [*Fiore*
591 *et al., 2002; Cooper et al., 2011*]. Within the western U.S., the model suggests strong
592 stratospheric impacts on the Sierra Nevada mountain range and Nevada Air
593 Basins, where monitoring sites are fairly sparse (Figure 13b). Measurements in
594 these rural areas would help improve our understanding of stratospheric influence
595 on $O_3$ air quality in nearby urban areas.

596

597 The bias-corrected estimates of median stratospheric impacts in surface air range
598 from 10–22, 8–13, and 3–8 ppbv in the West, Northeast, and Southeast, respectively
599 (Figure 13c). In the intermountain west, the stratospheric exchange can contribute
600 20-30% of the total measured $O_3$ averaged over April through June. The AM3
601 estimate for the western U.S. is approximately 30-50% higher than the estimates by
602 *Lelieveld and Dentener* [2000] and *Collins et al.* [2003], and a factor of 2 greater
603 than the estimate of *Fiore et al.* [2003].

Surface regions subject to a maximum stratospheric impact of 35-55 ppbv on MDA8 $O_3$ include Wyoming, Utah, Colorado, Southern California, Arizona, and New Mexico (Figure 13d), consistent with the case studies in Section 3. Although local emissions dominate surface $O_3$ pollution over the northeastern U.S. (Figure 13b), AM3 estimates a maximum stratospheric contribution of 30-45 ppbv at several scattered sites, supporting prior publications that deep STT can occur over this region [*Moody et al., 1998*; *Sprenger and Wernli, 2003*; *Hocking et al., 2007*; *Bourqui and Trepanier, 2010; Lefohn et al., 2011*]. *Thompson et al. and Pfister et al* [2007] estimate a 20-25% stratospheric contribution to the total tropospheric $O_3$ column over the northeastern U.S. in summer. Further process-oriented analysis of intensive measurements with a model is needed to confidently assess the influence of deep STT on surface $O_3$ air quality over this region.

### 5.2 Implications for Attaining Ozone Air Quality Standards

Next we assess the $O_3$ enhancements from stratospheric intrusions for the entire distribution of observed MDA8 $O_3$ over the intermountain west (Figure 14). Statistics of both original and bias-corrected AM3 estimates of the NA Background and the stratospheric contribution for each 10 ppbv bin of observed $O_3$ are shown. We focus on the bias-corrected estimates at the high end of the observed $O_3$ distribution, which has major implications for the NAAQS-setting process and health risk assessment associated with $O_3$ exposure.

Both NA background $O_3$ and its stratospheric component peak at the high-end of the observed $O_3$ distribution for the high-elevation sites across the intermountain west (Figure 14b) as well as for the AQS sites in the central western U.S. (Figure 14a). At high-elevation sites, $25^{th}$-$75^{th}$ percentiles of stratospheric contribution range from 14-25 ppbv when observed $O_3$ is 60-70 ppbv and increase to 17-40 ppbv in the 70-85

631 ppbv range. The median value of the stratospheric contribution at the AQS sites
632 primarily within EPA Region 8 (Figure 1) is approximately 10 ppbv lower as
633 compared to the high-elevation sites when observed $O_3$ is above 70 ppbv.
634
635 For relatively polluted areas, such as the Central Valley, Southern California and Las
636 Vegas, transport of stratospheric $O_3$ to the surface can mix with high levels of locally
637 produced $O_3$ pollution. At these areas (Figure S7), NA background and its
638 stratospheric component peak in the 60-80 ppbv range of observed $O_3$ and both
639 tend to decline by 2-5 ppbv when observed $O_3$ is in the 80-100 ppbv range. This
640 variability is more qualitatively consistent with earlier work for the eastern U.S. [*e.g.*
641 *Fiore et al., 2002; 2003*].
642
643 AM3 captures episodes of high-$O_3$ in excess of 70 ppbv at high-elevation western
644 U.S. sites. The maximum background MDA8 $O_3$ concentration can reach 60-75 ppbv
645 (bias-corrected) and in these cases is primarily driven by stratospheric $O_3$. In
646 contrast, two recent model estimates by Zhang et al [2011] and Emery et al [2011],
647 show that the NA background is always below 60-65 ppbv. The median value of NA
648 background when observed $O_3$ exceeds 70 ppbv is also ~10 ppbv greater in AM3
649 estimates.
650
651 Table 2 shows that AM3 captures accurately the observed $O_3$ values in excess of 60
652 ppbv at high-elevation sites, and estimates a total background contribution of 83%
653 and a North American anthropogenic contribution of 17%. The stratospheric
654 contribution and Asian pollution comprise 47% and 10% of the total background,
655 respectively. The dominant contribution from stratospheric $O_3$ and larger impacts
656 with increasing $O_3$ indicates a major role for stratospheric $O_3$ intrusions in driving
657 springtime surface high-$O_3$ events over the U.S. Mountain West, posing a major

658 challenge for attaining the NAAQS.

659 **6. Conclusions**

660 To determine the extent to which naturally occurring stratospheric $O_3$ intrusions
661 contribute to exceedances of the U.S. National Ambient Air Quality Standard
662 (NAAQS) for $O_3$, we analyzed a suite of satellite and *in situ* observations over the
663 western U.S. from April-June 2010 utilizing a global chemistry-climate model at
664 ~50x50 $km^2$ (GFDL AM3) [*Lin et al., 2012*]. While *Lefohn et al. [2001,2011] and*
665 *Langford et al. [2009, 2012*] have used observations and trajectory models to infer a
666 stratospheric influence on surface $O_3$ events, here we quantify that influence with a
667 new stratospheric $O_3$ tracer (Section 2.3) implemented in GFDL AM3 with fully
668 coupled stratosphere and troposphere chemistry [*Donner et al., 2011; Naik et al., in*
669 *prep*].
670
671 Our process-oriented analysis shows that AM3 reproduces the principal features of
672 deep stratospheric $O_3$ intrusions. Specifically, it captures the evolution of synoptic
673 conditions, the descent of stratospheric $O_3$ to the lower troposphere as evidenced by
674 its replication of the layered structures and sharp gradients observed in $O_3$ profiles
675 (Figures 5 and 8), and the development of high-$O_3$ events observed in surface air
676 (Figure 9). The good agreement builds confidence in the utility of AM3 for identifying
677 "exceptional stratospheric intrusion events" that elevate surface $O_3$ to values above
678 the NAAQS threshold [*U.S. EPA, 2007; Langford et al., 2009*]. The most significant
679 weakness of the model is a high surface $O_3$ bias of ~6 ppbv on average, and
680 occasionally up to 10-20 ppbv in daily maximum 8-hour average (MDA8) over the
681 Southwest during the intrusion events. We correct the AM3 estimate of stratospheric
682 $O_3$ contribution to account for this model bias by conservatively assuming that the
683 model overestimates at ground-based measurement sites are entirely driven by
684 excessive stratospheric $O_3$ influence (Section 4.2).

685

686 Thirteen stratospheric $O_3$ intrusion events, occurring approximately weekly from
687 April-June 2010 (Table 1), led directly to observed MDA8 $O_3$ above 60 ppbv, and
688 sometimes over the 75-ppbv NAAQS threshold, at surface sites. Several of these
689 events occurred in suburban areas of California and Colorado. This finding is in
690 notable contrast to prior work concluding that stratospheric influence in surface air is
691 rare [e.g. *Fiore et al., 2003*; *U.S. EPA, 2007*]. We show that transport of stratospheric
692 $O_3$ to the surface can drive a substantial portion of the observed synoptic variability
693 in western U.S. surface $O_3$ (Figures 4 and 11) and contributes more than $O_3$
694 produced from North American and Asian anthropogenic emissions (Table 2). During
695 four deep intrusion events (April 12-14, May 22-24, May 27-29, and June 7-8),
696 stratospheric influence accounts for 30-55 ppbv of $O_3$ in surface air (e.g. Figures 7
697 and 9), composing 50-60% of the total. These stratospheric intrusions elevated
698 background $O_3$ concentrations to MDA8 values of 60-75 ppbv. Both the background
699 $O_3$ concentration and its stratospheric component peak at the high-end of the
700 observed $O_3$ distribution over the U.S. Mountain West (Figure 14).

701

702 AM3 estimates of stratospheric impacts on springtime surface $O_3$ over the western
703 U.S. is generally higher on average, and up to 2-3 times greater during the intrusions,
704 than previous model estimates [*e.g. Lelieveld and Dentener 2000; Collins et al.,*
705 *2003*; *Fiore et al., 2003; Langford et al., 2012*]. While some of the discrepancies may
706 reflect interannual variability associated with ENSO and other factors (Section 3.1),
707 the major improvement of GFDL AM3 upon previous chemical transport models,
708 including its higher resolution and representation of stratospheric chemistry and
709 UT/LS dynamics, builds confidence in its estimates of extreme impacts from
710 stratospheric intrusions.

711

Our analysis implies that large stratospheric impacts may pose a major challenge for attaining the ozone NAAQS with domestic emission controls over the western U.S., particularly if a threshold value in the 60-70 ppbv range were to be adopted [U.S. EPA, 2010]. Some climate models project a higher contribution of stratospheric exchange to tropospheric $O_3$ under future climate scenarios, presumably due to stratospheric $O_3$ recovery and an accelerated stratospheric circulation in a warmer climate [e.g. *Collins et al., 2003; Austin and Wilson 2006; Stevenson et al., 2006; Hegglin and Shepherd, 2009; Zeng et al, 2010*]. Further analysis of long-term chemical and meteorological observations may reveal key connections between climate and stratospheric impacts on surface $O_3$ air quality.

**Acknowledgements:**

This work is supported by the Cooperative Institute for Climate Science (CICS) -- a collaboration between Princeton University and NOAA Geophysical Fluid Dynamics Laboratory (GFDL), and by the NASA Air Quality Applied Science Team (AQAST) (NNX12AF15G). Funding for the IONS-2010 field campaign was provided by NOAA ESRL Health of the Atmosphere Program, NASA Tropospheric Chemistry Program, U. S. Navy, Environment Canada and NOAA's National Air Quality Forecast Capability. Operations were facilitated by personnel from Joshua Tree National Park, Point Reyes National Seashore, Shasta State Historic Park, Point Sur State Historic Park, and the Naval Postgraduate School (NPS), Monterey. We are grateful to Zhiguo Zhang for help processing AQS data and to Paul Ginoux, Allen Lefohn, Bud Moxim, and Joe Pinto for discussions and comments on the manuscript.

## References:


Appenzeller, C. and Davies, H. C. (1992), Structure of stratospheric intrusions into the troposphere: Nature, 358 (6387), 570-572.

Alvarez II, R. J., C. J. Senff, A. O. Langford, et al (2011): Development and application of a compact, tunable, solid-state airborne ozone lidar system for boundary layer profiling, *J. Atmos. Oceanic Technol.*, doi: 10.1175/JTECH-D-10-05044.1.

Austin, J. and R. J. Wilson (2006), Ensemble simulations of the decline and recovery of stratospheric ozone, J. Geophys. Res., 111, D16314, doi:10.1029/2005JD006907

Austin, J. and R. J. Wilson (2010), Sensitivity of polar ozone to sea surface temperatures and halogen amounts, J. Geophys. Res., 115, D18303, doi:10.1029/2009JD013292.

Bourqui, M. S. and P.-Y. Trepanier (2010), Descent of deep stratospheric intrusions during the IONS August 2006 campaign: J. Geophys. Res., 115, D18301, doi:10.1029/2009JD013183

Browell, E. V., E. F. Danielsen, S. Ismail, G. L. Gregory, and S. M. Beck (1987), Tropopause fold structure determined from airborne lidar and in situ measurements, J. Geophys. Res., 92, 2112-2120.

Collins, W. J., et al. (2003), Effect of stratosphere-troposphere exchange on the future tropospheric ozone trend, J. Geophys. Res., 108, 8528, doi:10.1029/2002JD002617.

Cooper, O. R., et al. (2001), Trace gas signatures of the airstreams within North Atlantic cyclones: Case studies from the NARE'97 aircraft intensive, J. Geophys. Res., 106 (D6), 5437–5456, doi:10.1029/2000JD900574.

Cooper, O. R., et al. (2004), On the life cycle of a stratospheric intrusion and its dispersion into polluted warm conveyor belts, J. Geophys. Res., 109, D23S09, doi:10.1029/2003JD004006.

Cooper, O. R., et al. (2005), Direct transport of mid-latitude stratospheric ozone into the lower troposphere and marine boundary layer of the tropical Pacific Ocean, J. Geophys. Res., 110, D23310, doi:10.1029/2005JD005783.

Cooper, O. R, et al. (2011), Measurement of western U.S. baseline ozone from the surface to the tropopause and assessment of downwind impact regions, J. Geophys. Res., doi:10.1029/2011JD016095

Danielsen, E. F. (1968), Stratospheric-tropospheric exchange based on radioactivity, ozone and potential vorticity, J. Atmos. Sci., 25, 502–518.

Donner, L. J., Wyman, B. L., Hemler, R. S. et al (2011), The Dynamical Core, Physical Parameterizations, and Basic Simulation Characteristics of the Atmospheric Component AM3 of the GFDL Global Coupled Model CM3. Journal of Climate, 24, 3484–3519, doi: 10.1175/2011JCLI3955.1

Emery, C., Jung, J., Downey, N., Johnson, J., Jimenez, M., Yarwood, G., Morris, R. (2011), Regional and Global Modeling Estimates of Policy Relevant Background Ozone over the United States, Atmos. Environ., 47, 206-217, doi: 10.1016/j.atmosenv.2011.11.012

Emmons, L. K., et al. (2003), Budget of tropospheric ozone during TOPSE from two chemical transport models, J. Geophys. Res., 108(D8), 8372, doi:10.1029/2002JD002665

775 Emmons, L.K., et al. (2010), Description and evaluation of the Model for Ozone and Related
776 chemical Tracers, version 4 (MOZART-4). Geosci. Model Dev., 3, 43-67,
777 doi:10.5194/gmd-3-43-2010
778 Felker, S. R., J. L. Moody, A. J. Wimmers, G. Osterman, and K. Bowman (2011), A multi-sensor
779 upper tropospheric ozone product (MUTOP) based on TES ozone and GOES water vapor:
780 derivation, Atmos. Chem. Phys., 11, 6515-6527, doi:10.5194/acp-11-6515-2011
781 Fiore, A. M., D. J. Jacob, I. Bey, R. M. Yantosca, B. D. Field, A. C. Fusco, and J. G.Wilkinson
782 (2002), Background ozone over the United States in summer: Origin, trend, and
783 contribution to pollution episodes, J. Geophys. Res.,107(D15), 4275,
784 10.1029/2001JD000982.
785 Fiore, A., Jacob, D.J., Liu, H., Yantosca, R.M., Fairlie, T.D., Li, Q. (2003), Variability in surface
786 ozone background over the United States: implications for air quality policy. J. Geophys.
787 Res. 108 (D24), 4787, doi:10.1029/2003JD003855.
788 Hegglin, M.I, and T.G. Shepherd (2009), Large climate-induced changes in ultraviolet index and
789 stratosphere-to-troposphere ozone flux, Nature Geoscience, 2, 687-691,
790 doi:10.1038/NGEO604.
791 Hess, P. G., and J.-F. Lamarque (2007), Ozone source attribution and its modulation by the
792 Arctic oscillation during the spring months, J. Geophys. Res., 112, D11303,
793 doi:10.1029/2006JD007557.
794 Hocking, W. K. et al (2007), Detection of stratospheric ozone intrusions by windprofiler
795 radars, *Nature*, *450*, 281–284.
796 Horowitz, L.W. et al (2003), A global simulation of tropospheric ozone and related tracers:
797 description and evaluation of MOZART, version 2. J. Geophys. Res., 108, D24,
798 doi.10.1029/2002JD002853.
799 Holton, J. R., P. H. Haynes, E. M. McIntyre, A. R. Douglass, R. B. Rood, and L. Pfister (1995),
800 Stratosphere-troposphere exchange, Rev. Geophys., 33, 403–439.
801 Hsu, J., M. J. Prather, and O. Wild (2005), Diagnosing the stratosphere-to-troposphere flux of
802 ozone in a chemistry transport model, J. Geophys. Res., 110, D19305,
803 doi:10.1029/2005JD006045
804 Hsu, J., and M. J. Prather (2009), Stratospheric variability and tropospheric ozone, J. Geophys.
805 Res., 114, D06102, doi:10.1029/2008JD010942.
806 Hudman, R. C., et al. (2004), Ozone production in transpacific Asian pollution plumes and
807 implications for ozone air quality in California, J. Geophys. Res., 109, D23S10,
808 doi:10.1029/2004JD004974
809 James, P., A. Stohl, C. Forster, S. Eckhardt, P. Seibert, and A. Frank, A 15-year climatology of
810 stratosphere-troposphere exchange with a Lagrangian particle dispersion model: 2. Mean
811 climate and seasonal variability, *J. Geophys. Res.*, *108* (D12), 8522,
812 doi:10.1029/2002JD002639, 2003
813 Johnson, W. B., and W. Viezee (1981), Stratospheric ozone in the lower troposphere: I.
814 presentation and interpretation of aircraft measurement, Atmos. Environ., 15, 1309– 1323.
815 Koumoutsaris S., I. Bey, S. Generoso, and V. Thouret (2008) Influence of El Nino-Southern

816 Oscillation on the interannual variability of tropospheric ozone in the northern mid-latitudes,
817 J. Geophys. Res., 113, D19301, doi:10.1029/2007JD00975.
818 Lamarque, J. - F. and P. G. Hess (2004), Arctic Oscillation modulation of the Northern
819 Hemisphere spring tropospheric ozone, Geophys. Res. Lett., 31, L06127,
820 doi:10.1029/2003GL019116.
821 Langford, A. O., C. D. Masters, M. H. Proffitt, E. Y. Hsie, and A. F. Tuck (1996), Ozone
822 measurements in a tropopause fold associated with a cut-off low system, Geophysical
823 Research Letters, 23(18), 2501-2504, doi:10.1029/96GL02227
824 Langford, A.O., T.J. O'Leary, C.D. Masters, K.C. Aikin, M. H. Proffitt (1998), Modulation of middle
825 and upper tropospheric ozone at northern midlatitudes by the El Niño/Southern Oscillation,
826 Geophys., Res. Lett., 25, 2667-2670, doi:10.1029/98GL01909
827 Langford, A.O., K.C. Aikin, C.S. Eubank, and E.J. Williams (2009) Stratospheric contribution to
828 high surface ozone in Colorado during springtime, Geophys. Res. Lett. 36, L12801,
829 doi:10.1029/2009GL038367.
830 Langford, A. O., et al (2012), Stratospheric influence on surface ozone in the Los Angeles area
831 during late spring and early summer of 2010, *J. Geophys. Res.*, *117*, D00V06,
832 doi:10.1029/2011JD016766.
833 Lefohn, A. S., S. J. Oltmans, T. Dann, and H. B. Singh (2001), Present-day variability of
834 background ozone in the lower troposphere, J. Geophys. Res., 106(D9), 9945–9958,
835 doi:10.1029/2000JD900793.
836 Lefohn, A.S., et al. (2011), The importance of stratospheric-tropospheric transport in affecting
837 surface ozone concentrations in the western and northern tier of the United States, Atmos.
838 Environ, 45 (28), 4845-4857, doi:10.1016/j.atmosenv.2011.06.014
839 Lelieveld, J., and F. J. Dentener (2000), What controls tropospheric ozone?, *J. Geophys.*
840 *Res.*,*105 (D3)*, 3531–3551, doi:10.1029/1999JD901011
841 Levy, H., J. D. Mahlmann, W. J. Moxim, and S. C. Liu (1985), Tropospheric ozone: The role of
842 transport, J. Geophys. Res., 90 (D2), 3753–3772, doi:10.1029/JD090iD02p03753
843 Liang, Q., et al. (2007), Summertime influence of Asian pollution in the free troposphere over
844 North America, J. Geophys. Res., 112, D12S11, doi:10.1029/2006JD007919.
845 Lin, M., et al. (2012), Transport of Asian ozone pollution into surface air over the western United
846 States in spring, *J. Geophys. Res.*, *117*, D00V07, doi:10.1029/2011JD016961.
847 McDonald-Buller Elena C., et al (2011), Establishing Policy Relevant Background (PRB) Ozone
848 Concentrations in the United States, Environmental Science & Technology, 45 (22), 9484-
849 9497
850 McLinden, C. A., S. C. Olsen, B. Hannegan, O. Wild, M. J. Prather, and J. Sundet (2000),
851 Stratospheric ozone in 3-D models: A simple chemistry and the cross-tropopause flux, J.
852 Geophys. Res.,105(D11), 14,653–14,665, doi:10.1029/2000JD900124.
853 Moody, J. L., J. W. Munger, A. H. Goldstein, D. J. Jacob, and S. C. Wofsy (1998), Harvard
854 Forest regional-scale air mass composition by Patterns in Atmospheric Transport History
855 (PATH), J. Geophys. Res., 103(D11), 13,181–13,194, doi:10.1029/98JD00526.
856 Monks, P. S., A review of the observations and origins of the spring ozone maximum, *Atmos.*

*Environ.*, *34*, 3545–3561, 2000.

Moss, R. H., et al (2010), The next generation of scenarios for climate change research and assessment, Nature 463, 747-756, doi:10.1038/nature08823

National Research Council (NRC) (2009), *Global Sources of Local Pollution: An Assessment of Long-Range Transport of Key Air Pollutants to and From the United States*, 248 pp., Nat. Acad., Washington, D. C.

Neuman J. A., et al (2012), Observation of ozone transport from the free troposphere to the Los Angeles basin, J. Geophys. Res., 117, D00V09, doi:10.1029/2011JD016919

Pfister, G., A.M. Thompson, L.K. Emmons, P.G. Hess, J.-F. Lamarque, Y.E. Yorks (2008), Analysis of the Summer 2004 Ozone Budget over the U.S. using IONS observations and MOZART-4 simulations, J. Geophys. Res., VOL. 113, D23306, doi:10.1029/2008JD010190.

Prather, M., et al. (2001), *Atmospheric chemistry and greenhouse gases, in Climate Change 2001: The Scientific Basis. Third Assessment Report of the Intergovernmental Panel on Climate Change*, edited by J. T. Houghton et al., pp. 239–287, Cambridge Univ. Press, Cambridge, U. K.

Prather, M. J., X. Zhu, Q. Tang, J. Hsu, and J. L. Neu (2011), An atmospheric chemist in search of the tropopause, J. Geophys. Res., 116, D04306, doi:10.1029/2010JD014939.

Roelofs, G.-J., and J. Lelieveld (1997), Model study of the influence of cross-tropopause $O_3$ transports on tropospheric $O_3$ levels, Tellus, Ser. B, 49, 38–55, 1997.

Roelofs, G. J., et al. (2003), Intercomparison of tropospheric ozone models: Ozone transport in a complex tropopause folding event, J. Geophys. Res., 108(D12), 8529, doi:10.1029/2003JD003462.

Shapiro, M. A. (1980), Turbulent mixing within tropopause folds as a mechanism for the exchange of chemical constituents between the stratosphere and troposphere, J. Atmos. Sci., 37, 994–1004.

Sprenger, M., and H. Wernli (2003), A northern hemispheric climatology of cross-tropopause exchange for the ERA15 time period (1979–1993), J. Geophys. Res., 108(D12), 8521, doi:10.1029/2002JD002636.

Stevenson, D. S., et al. (2006), Multimodel ensemble simulations of present-day and near-future tropospheric ozone, J. Geophys. Res., 111, D08301, doi:10.1029/2005JD006338

Stohl, A., and T. Trickl (1999), A textbook example of long-range transport: Simultaneous observation of ozone maxima of stratospheric and North American origin in the free troposphere over Europe, J. Geophys. Res., 104, 30,445– 30,462

Stohl, A., et al. (2003), Stratosphere-troposphere exchange: A review, and what we have learned from STACCATO, J. Geophys. Res., 108(D12), 8516, doi:10.1029/2002JD002490.

Susskind, J., C. D. Barnet, and J. M. Blaisdell (2003), Retrieval of atmospheric and surface parameters from AIRS/AMSU/HSB data in the presence of clouds, IEEE Trans. Geosci. Remote Sens., 41, 390–409

Tarasick, D. W., et al. (2007), Comparison of Canadian air quality forecast models with tropospheric ozone profile measurements above mid-latitude North America during the IONS/ICARTT Campaign: Evidence for stratospheric input, J. Geophys. Res., 112,

898 D12S22, doi:10.1029/2006JD007782.
899 Terao, Y., J. A. Logan, A. R. Douglass, and R. S. Stolarski (2008), Contribution of stratospheric
900 ozone to the interannual variability of tropospheric ozone in the northern extratropics, J.
901 Geophys. Res., 113, D18309, doi:10.1029/2008JD009854.
902 Thompson, A. M., et al. (2007), Intercontinental Chemical Transport Experiment Ozonesonde
903 Network Study (IONS) 2004: 2. Tropospheric ozone budgets and variability over
904 northeastern North America, *J. Geophys. Res.*, *112*, D12S13, doi:10.1029/2006JD007670.
905 U.S. Environmental Protection Agency [2006], Air Quality Criteria for Ozone and Related
906 Photochemical Oxidants (2006 Final), U.S. Environmental Protection Agency, Washington,
907 DC, EPA/600/R-05/004aF-cF.
908 U.S. Environmental Protection Agency [2007], Treatment of data influenced by exceptional
909 events, Federal Register, 72 (55), 13560-13581.
910 U.S. Environmental Protection Agency [2010], National Ambient Air Quality Standards for Ozone,
911 Federal Register, 75 (11), 2938-3052.
912 World Health Organization (2005), WHO air quality guidelines global update, report on a working
913 group meeting, Bonn, Germany, 18–20 October, 2005, *Rep. E87950*, 25 pp., Geneva.
914 Wild O., X. Zhu, and M. Prather (2000), Fast-J: Accurate simulation of in- and below-cloud
915 photolysis in tropospheric chemical models, J. Atmos. Chem., 37 (3), 245-282,
916 doi:10.1023/A:1006415919030
917 Wild, O., et al. (2007), Modeling the global tropospheric ozone budget: exploring the variability in
918 current models, Atmos. Chem. Phys., 7, 2643-2660, doi:10.5194/acp-7-2643-2007.
919 Wimmers, A. J., J. L. Moody, E. V. Browell, J. W. Hair, W. B. Grant, C. F. Butler, M.A. Fenn, C. C.
920 Schmidt, J. Li, and B. A. Ridley (2003), Signatures of tropopause folding in satellite
921 imagery, J. Geophys. Res., 108(D4), 8360, doi:10.1029/2001JD001358.
922 Zhang, L., et al. (2011), Improved estimate of the policy-relevant background ozone in the United
923 States using the GEOS-Chem global model with $1/2^{o}$x$2/3^{o}$ horizontal resolution over North
924 America, Atmos. Environ., 45 (37), doi:10.1016/j.atmosenv.2011.07.054
925 Zeng, G., O. Morgenstern, P. Braesicke, and J. A. Pyle (2010), Impact of stratospheric ozone
926 recovery on tropospheric ozone and its budget, Geophys. Res. Lett., 37, L09805,
927 doi:10.1029/2010GL042812.

**Table 1: Stratospheric intrusion events contributing to surface ozone episodes during April-June 2010**

| Events | Synoptic conditions in satellite imagery | Descent captured in ozonesondes/lidar | Major surface impact regions |
|---|---|---|---|
| Apr. 6-7 | AIRS * | Not measured | Colorado, New Mexico (Fig. 11) |
| Apr. 9-10 | AIRS * | Not measured | Wyoming (Fig. 11) |
| Apr. 12-14[+] | AIRS (Fig. S1) | Not measured | Spread across Mountain West (Figs. 9-10) |
| Apr. 21-23 | AIRS * | Not measured | Colorado, Nevada (Fig. 11) |
| Apr. 28-29 | AIRS * | Not measured | Colorado, Wyoming (Fig. 11) |
| May 11-13 | AIRS/GOES-West* | Langford et al [2012] | Arizona, New Mexico, W. Texas (Fig. 11) |
| May 17-20 | AIRS (Lin et al.,2012) | Lin et al., [2012] | Wyoming (Fig. 11) |
| May 22-24 | AIRS/GOES-West (Fig. S2) | Figs. 8 and S3 | Colorado and New Mexico (Fig. 9) |
| May 27-29 | AIRS/GOES-West (Fig. S4) | Fig. 5 | California, Nevada, Arizona (Fig. 7) |
| Jun. 7-8 | AIRS/GOES-West (Fig. 2) | Fig. 4 | Idaho, Utah, Wyoming (Fig. 4) |
| Jun. 9-14 | AIRS/GOES-West (Fig. 2) | Fig. 4 | Spread in Southwest (Figs. 4) |
| Jun. 16-17 | AIRS/GOES-West* | Lin et al., [2012] | Colorado (Fig. 11) |
| Jun. 22-23 | AIRS* | Not measured | Colorado (Fig. 11) |

+Gray shading denotes case studies in Sections 3.2-3.4
*Data not shown

**Table 2 MDA8 ozone concentrations (ppbv) in surface air averaged over 15 high-elevation sites across the U.S. Mountain West for April-June 2010**

| | Mean | Mean for days > 60 ppbv |
|---|---|---|
| Total observed | 55.3 ± 8.3 | 65.1 ± 4.4 |
| Total modeled | 61.0 ± 8.6 | 66.0 ± 8.3 |
| NA anthropogenic | 11.0 ± 5.0 | 11.6 ± 5.3 |
| Total background[+] | 50.0 ± 10.6 | 54.5 ± 10.6 |
| Asian anthropogenic* | 4.7 ± 2.4 | 5.3 ± 2.6 |
| Stratospheric | 22.3 ± 11.5 | 25.4 ± 12.3 |

+Includes the contribution from Asian pollution and stratospheric $O_3$
*Based on AM3 simulations as described by *Lin et al* [2012]

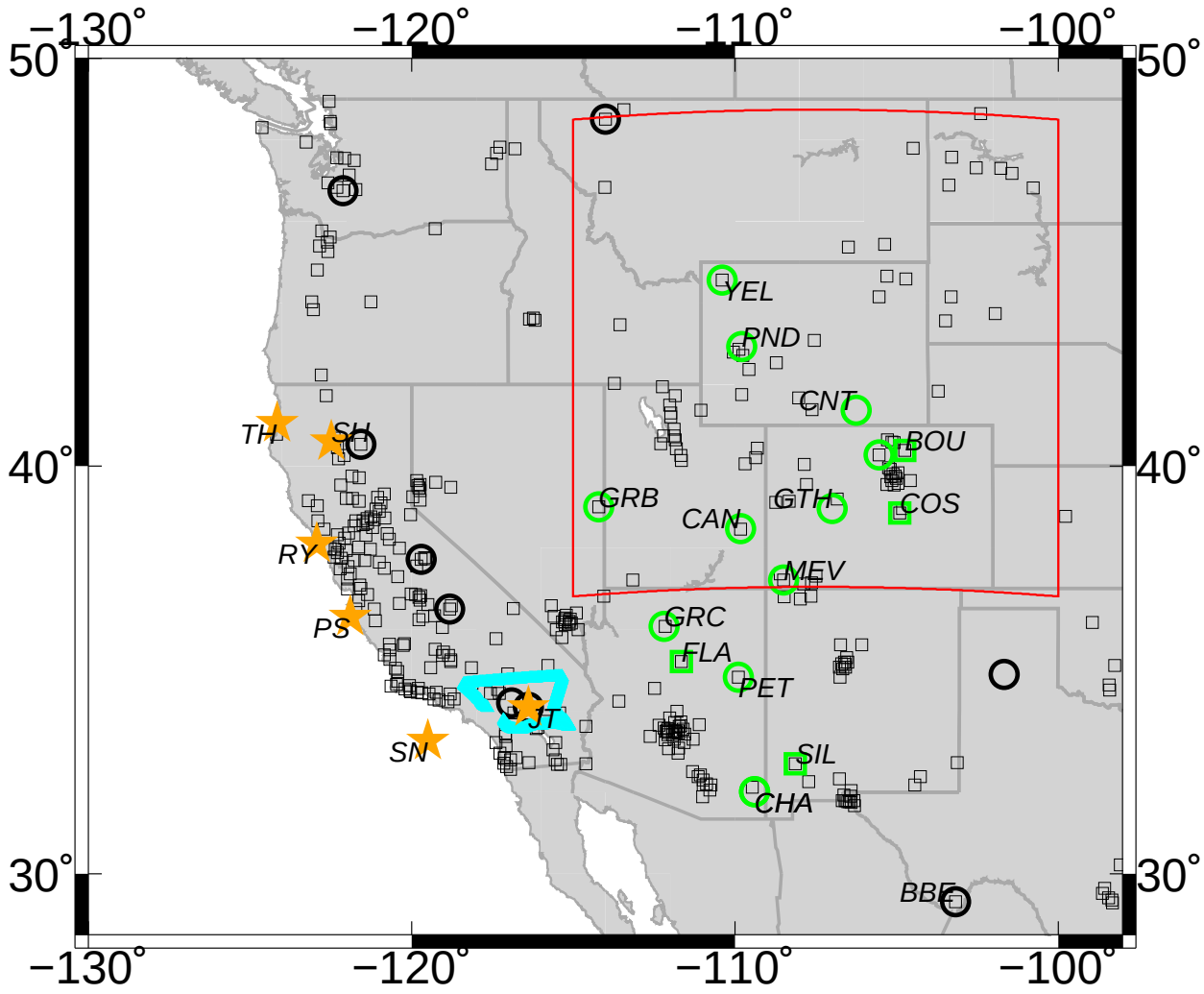


Figure 1. Map showing locations of six ozonesonde sites (orange stars) in California, flight path of an aircraft-based ozonelidar on May 23 (solid cyan, Figure 8), and surface monitoring sites from CASTNet (circles) and AQS (squares). The green symbols indicate 15 select sites analyzed in Figures 12b and 14b. The red box encloses the AQS sites analyzed in Figures 12a and 14a. These AQS sites are primarily located in EPA Region 8 (Utah, Colorado, Wyoming, Montana, North and South Dakota).

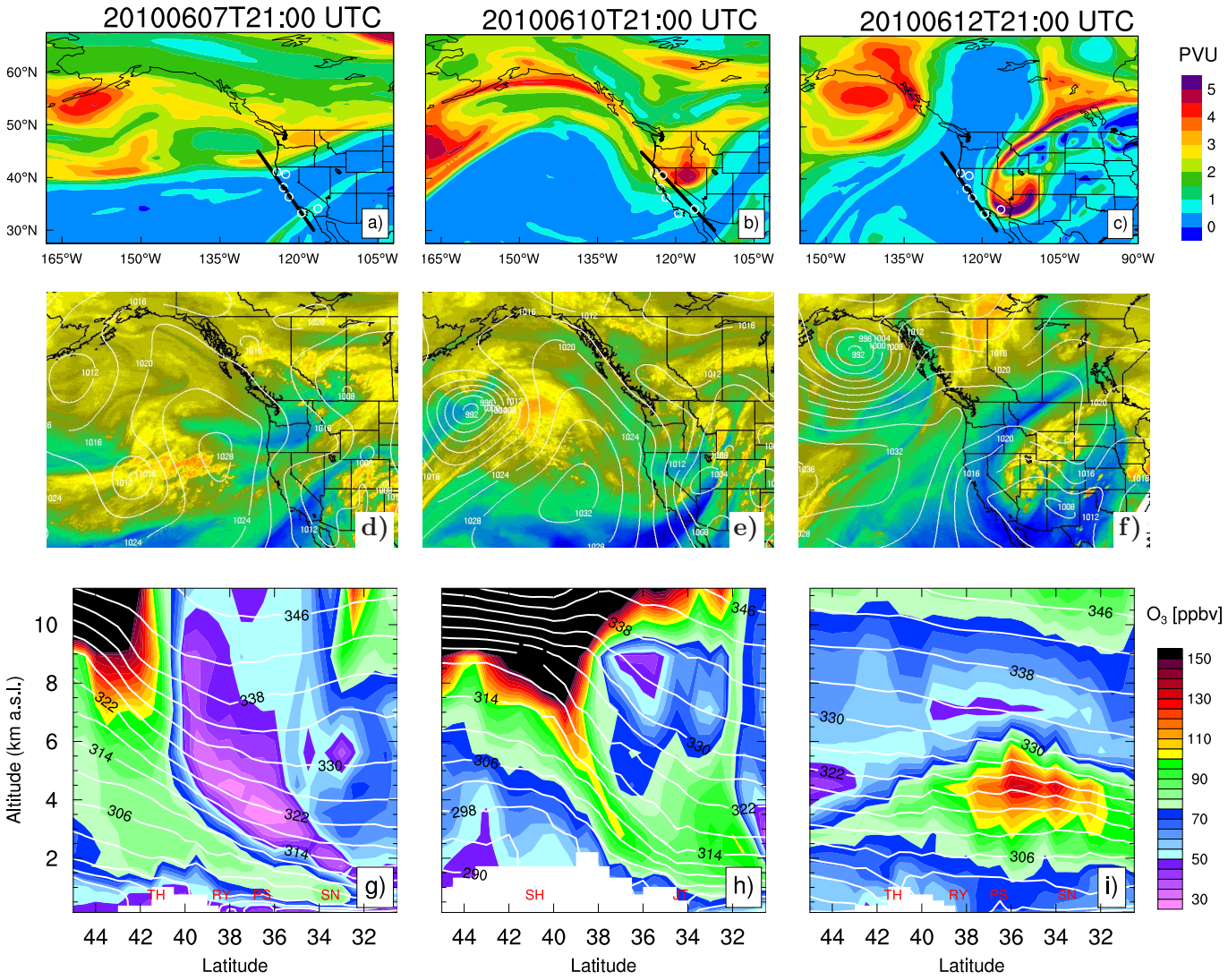


Figure 2. Synoptic conditions during June 7-14 intrusions: (a-c) AM3 250 hPa potential vorticity; (d-f) GOES-West water vapor images (with mean sea level pressure contours), which indicate relative humidity in the mid- to upper troposphere, with reds and yellows indicating moist air and blues and greens indicating drier air; (g-i) Latitude-height curtain plots of AM3 ozone distributions (shading) and isentropic surfaces (contoured in K) along the coastal or inland transects (thick lines) in a-c. White circles in a-c and red letters in g-i denote locations of ozonesondes.

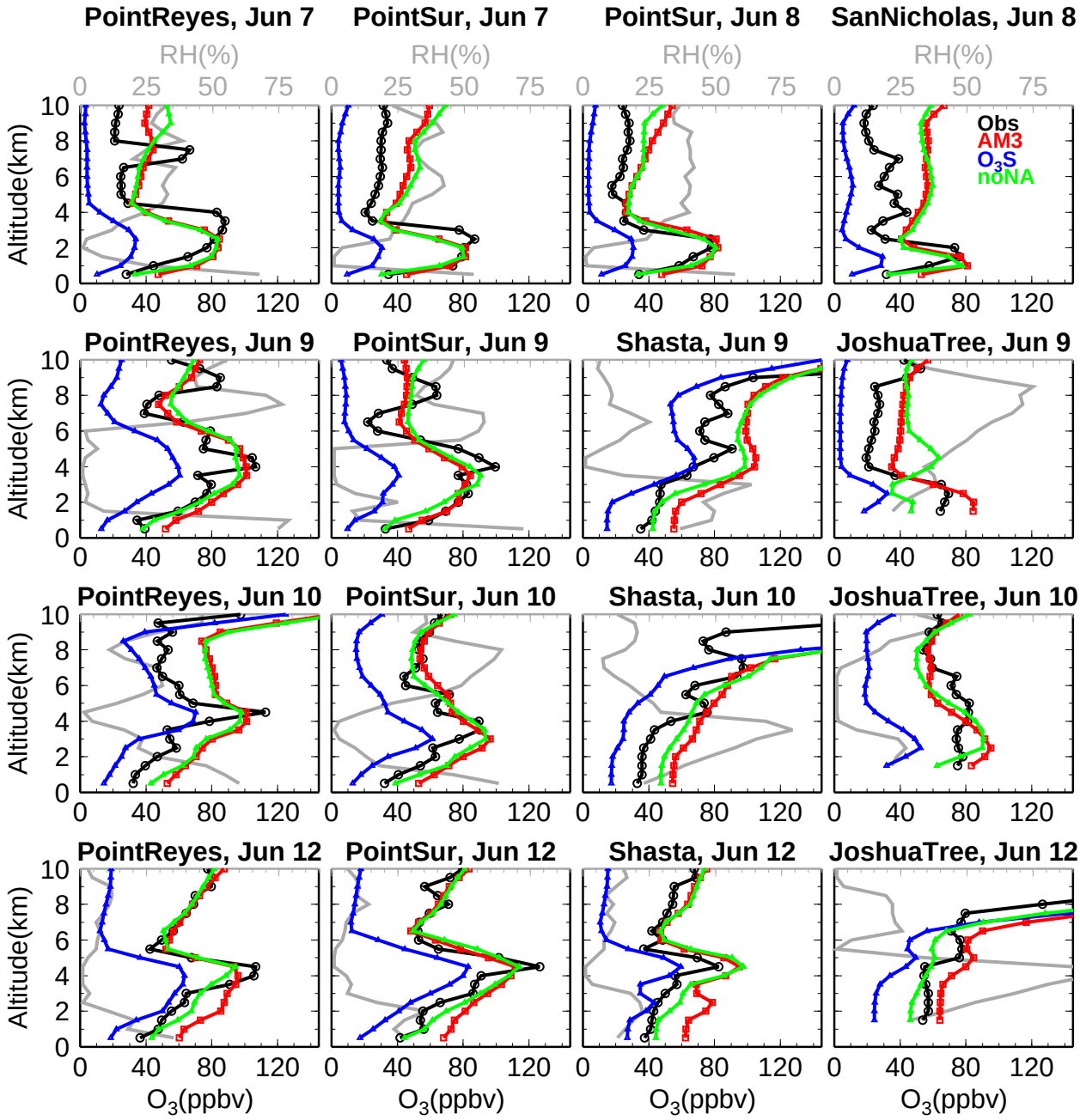


Figure 3. Ozone profiles at the June 7-12 soundings as observed (black) and estimated (red) by the GFDL AM3 model. Also shown are observed relative humidity (gray), AM3 stratospheric $O_3$ tracer (blue) (Section 2.3), and estimated ozone with North American anthropogenic emissions turned off (green) (Section 2.2). Model results have been interpolated to sonde pressure and averaged over 0.5-km altitude bins.

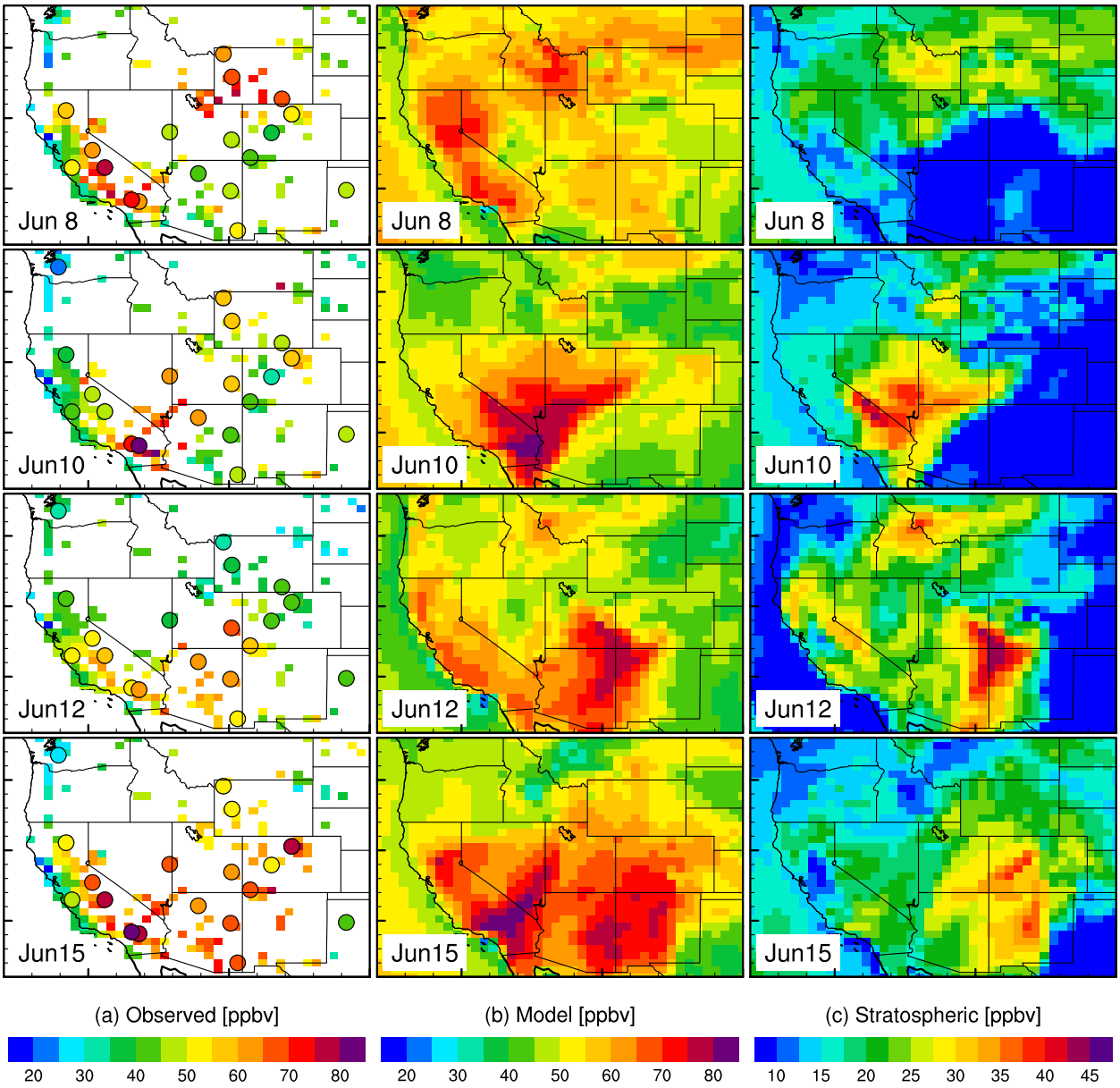


Figure 4. Daily maximum 8-hour average ozone in surface air from June 8-15: (a) observed at CASTNet sites (circles) and AQS averaged over the 0.5° by 0.625° grid (squares), (b) simulated by the GFDL AM3 model and (c) the stratospheric contribution (on a different color scale).

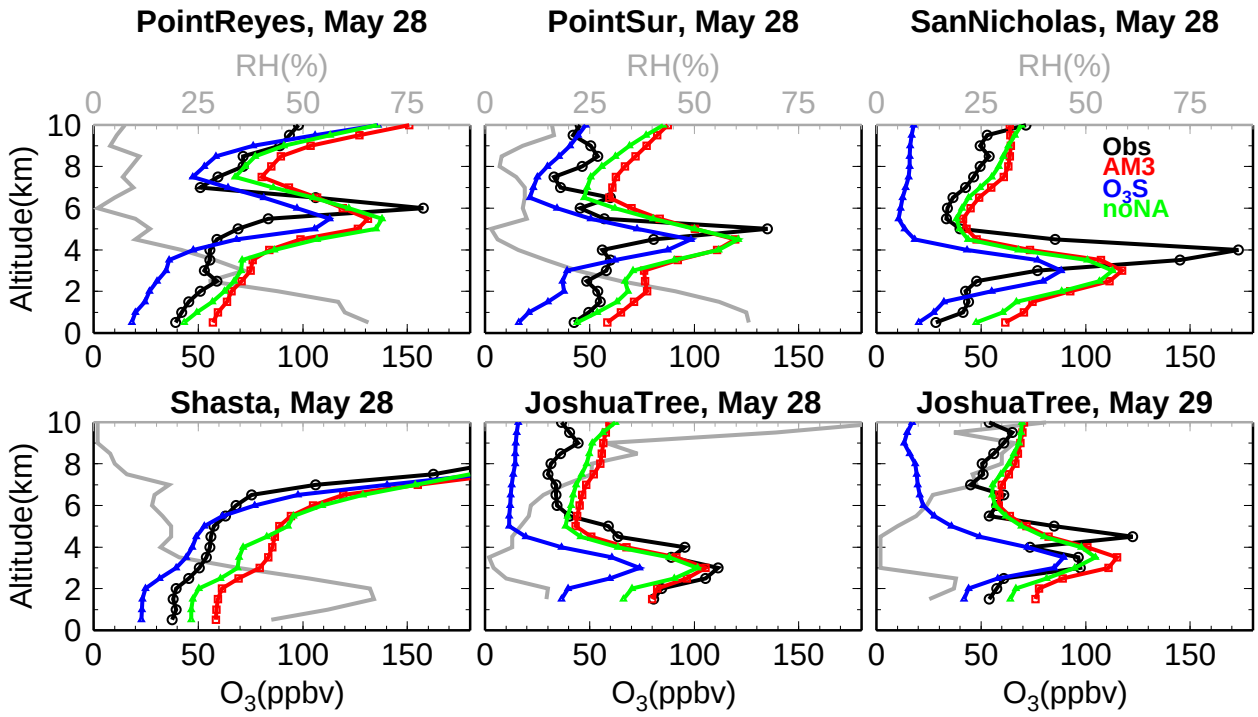


Figure 5. Same as Figure 3, but for the May 28-29 intrusion.

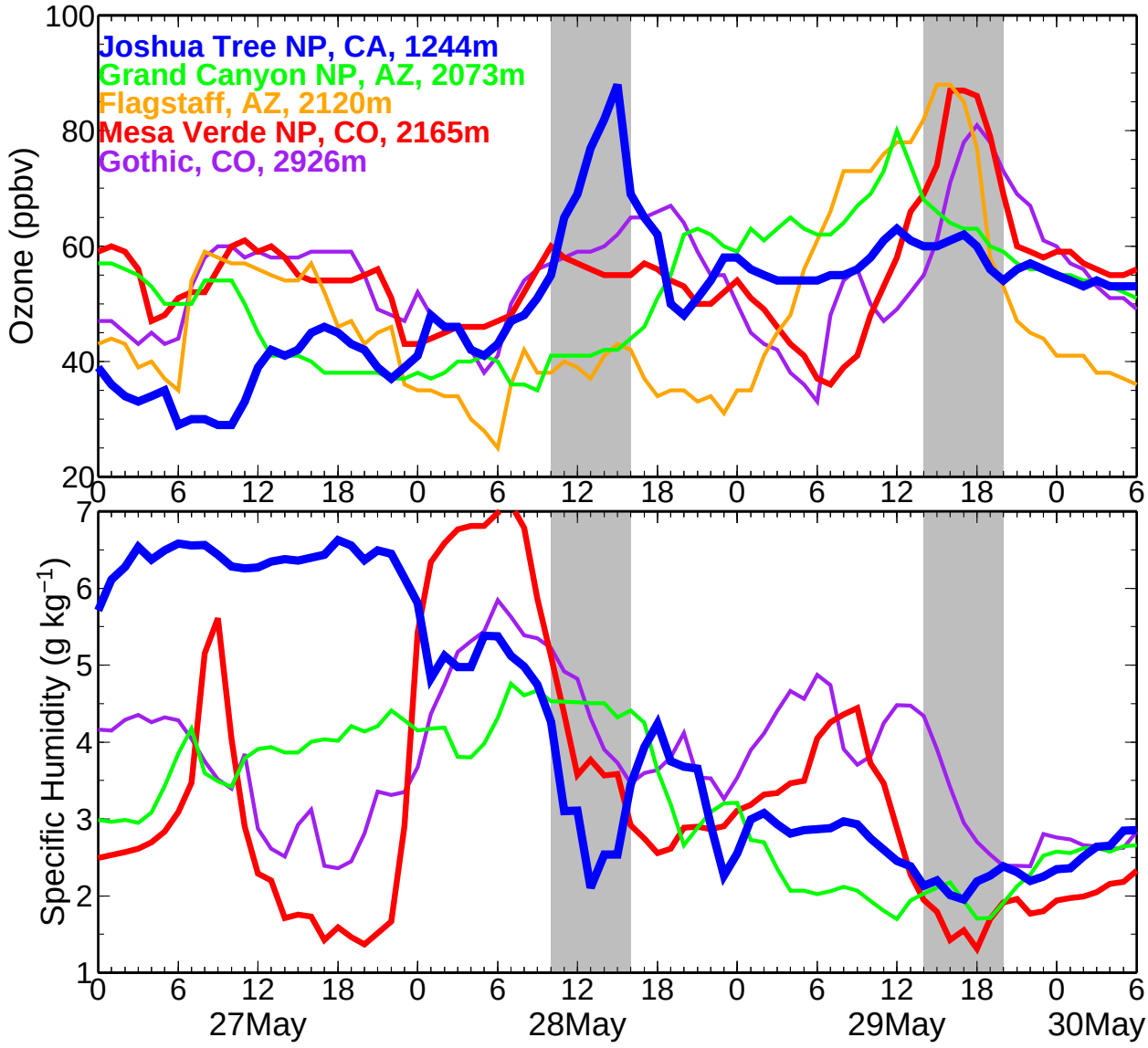


Figure 6. Time series of observed hourly ozone mixing ratios and specific humidity in surface air at the indicated stations (Figure 7b) from May 27-30, 2010. Note that humidity is not measured at Flagstaff. The gray shading masks the period at local time when the boundary layer is well mixed.

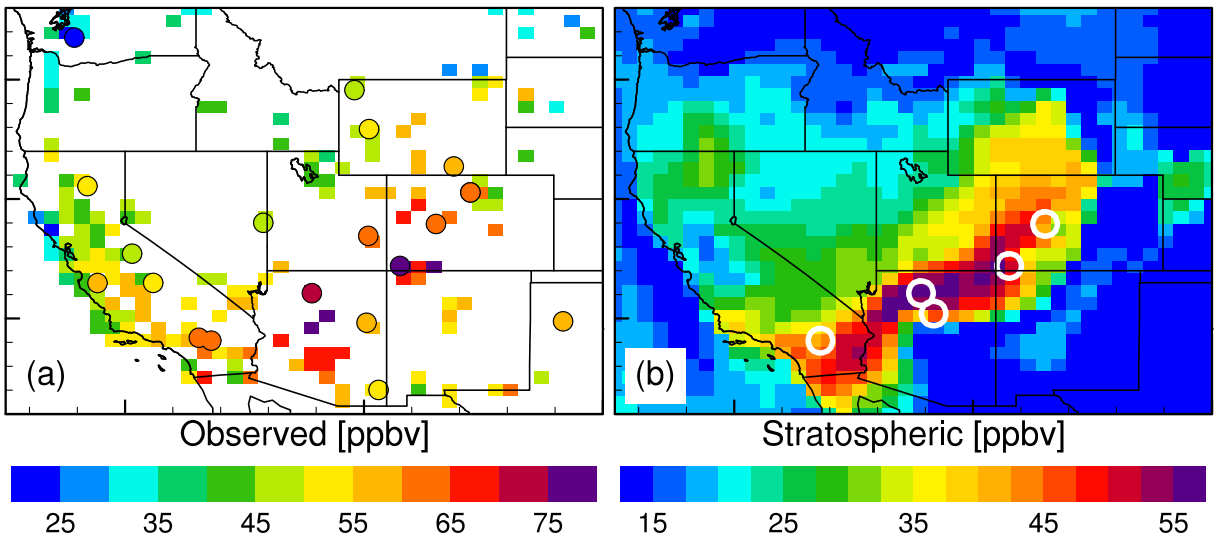


Figure 7. Daily maximum 8-hour average ozone in surface air on May 29, 2010, as (a) observed and (b) estimated by AM3 from the stratospheric intrusion. The white circles in (b) denote the surface sites experiencing drier conditions on the afternoon as shown in Figure 6.

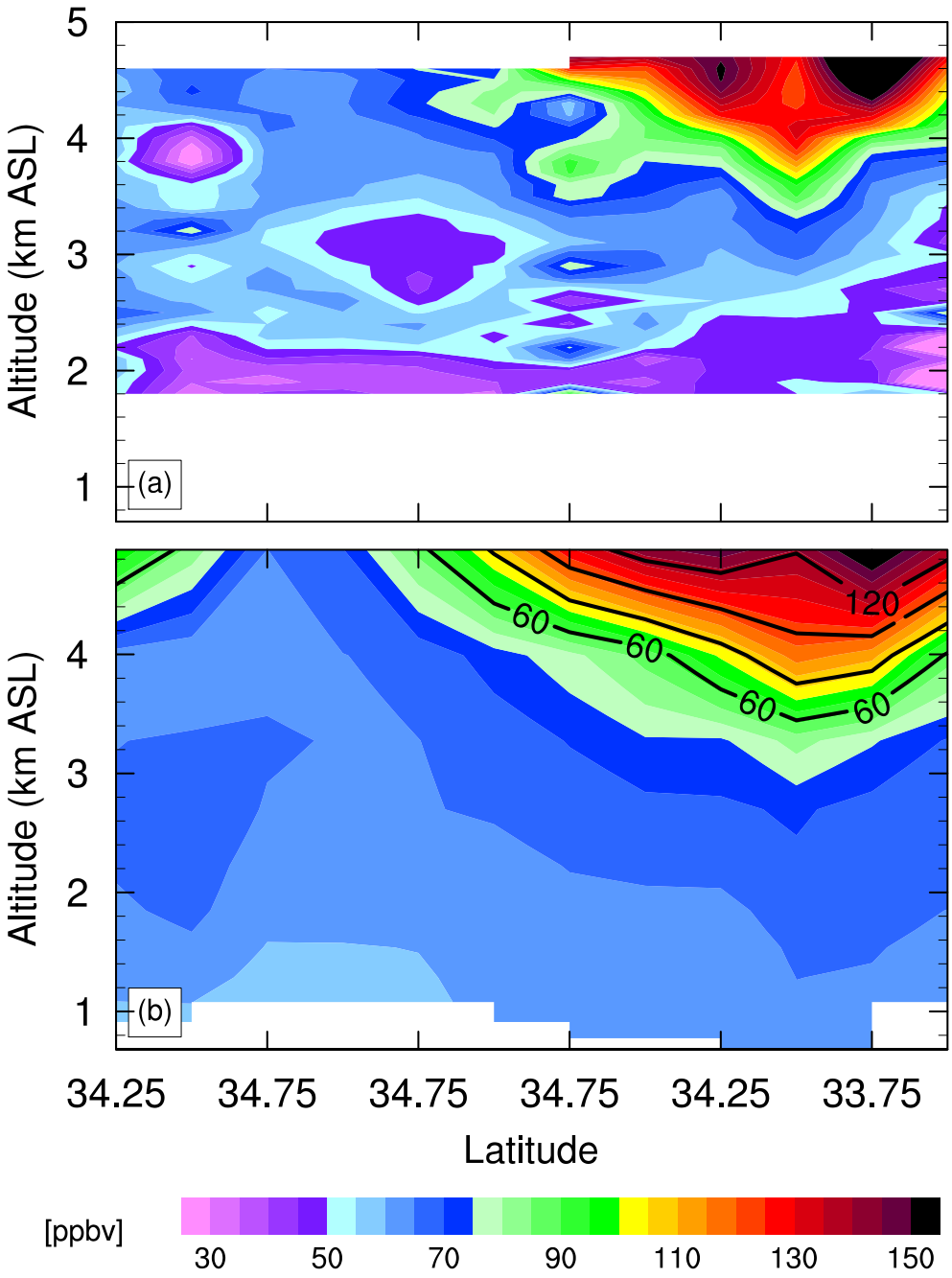


Figure 8. Latitude-height curtain plots of ozone mixing ratios over Southern California for May 23 as (a) measured by an aircraft-based lidar (Figure 1) and (b) simulated by the GFDL AM3 model. Also shown is AM3 stratospheric ozone tracer contoured every 20 ppbv starting at 60 ppbv.

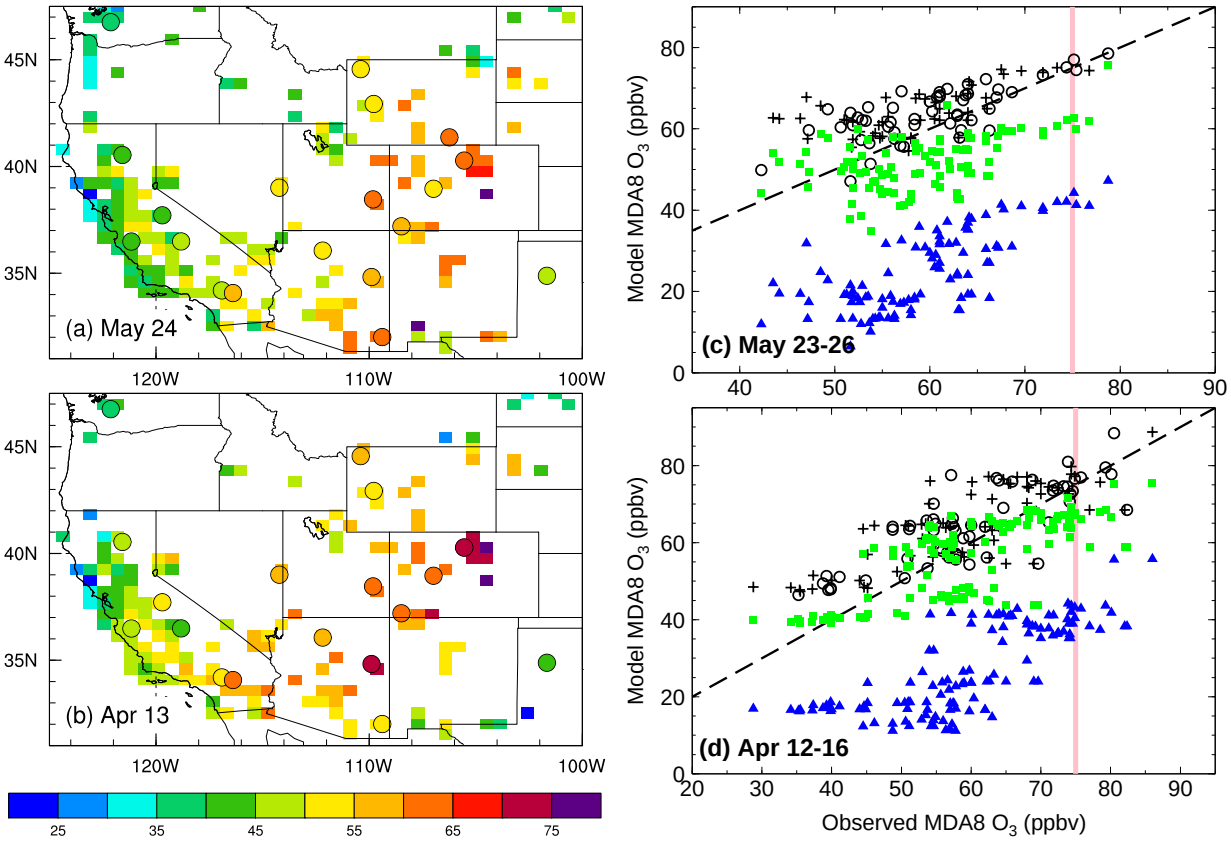


Figure 9. (a-b) Observed daily maximum 8-hour average (MDA8) ozone in surface air on May 24 and April 13. (c-d) Scatter plots of observed versus simulated MDA8 ozone (black) as well as corresponding contributions from stratospheric intrusions (blue) and NA background (green, Section 2.2) at 25 sites where peak MDA8 values exceed 60 ppbv during May 23-26 and April 12-16. Crosses indicate 9 urban and suburban sites located in Denver, Boulder, and Colorado Springs. Also shown is the 1:1 line and the NAAQS threshold.

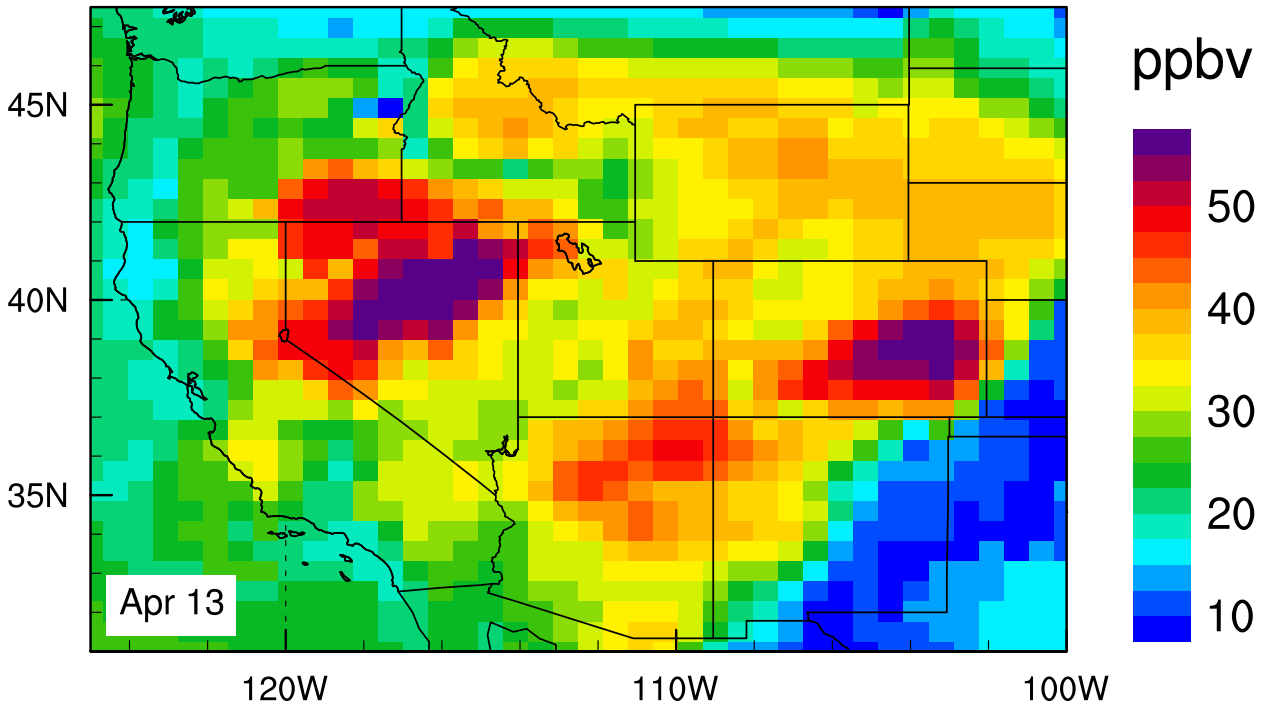


Figure 10. Daily maximum 8-hour average concentrations of stratospheric ozone tracer in the model surface layer on April 13, 2010.

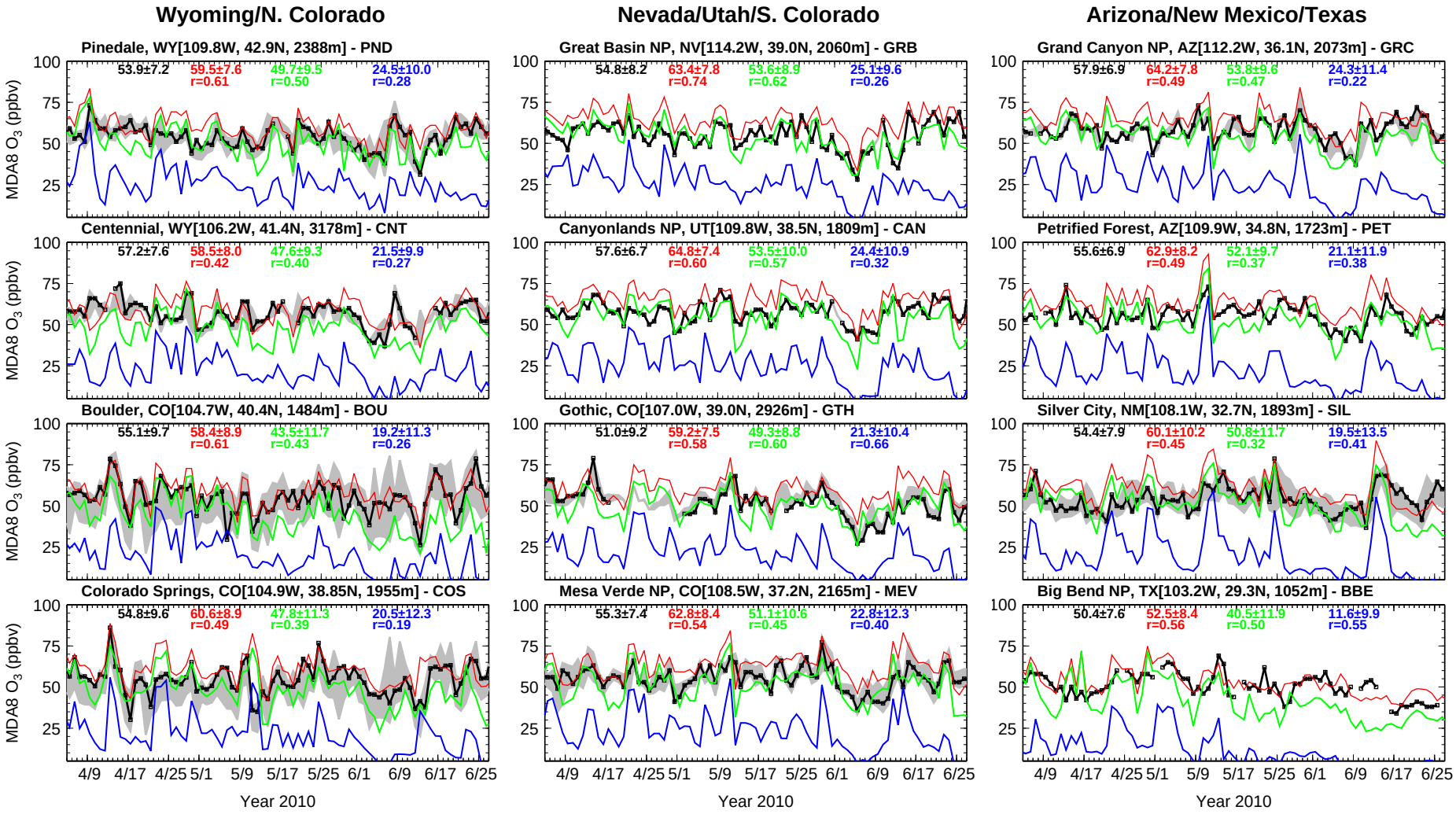


Figure 11. Time series of daily maximum 8-hour average $O_3$ in surface air at western U.S. sites (Fig. 1) for April through June 2010 as observed (black) and simulated (red) by the GFDL AM3 model. The gray shading represents range of observed $O_3$ available ∼100 km from the indicated site. Also shown are the model estimates for NA background (green) and the stratospheric contribution (blue), mean±standard deviations, and the model correlation coefficients with observations.

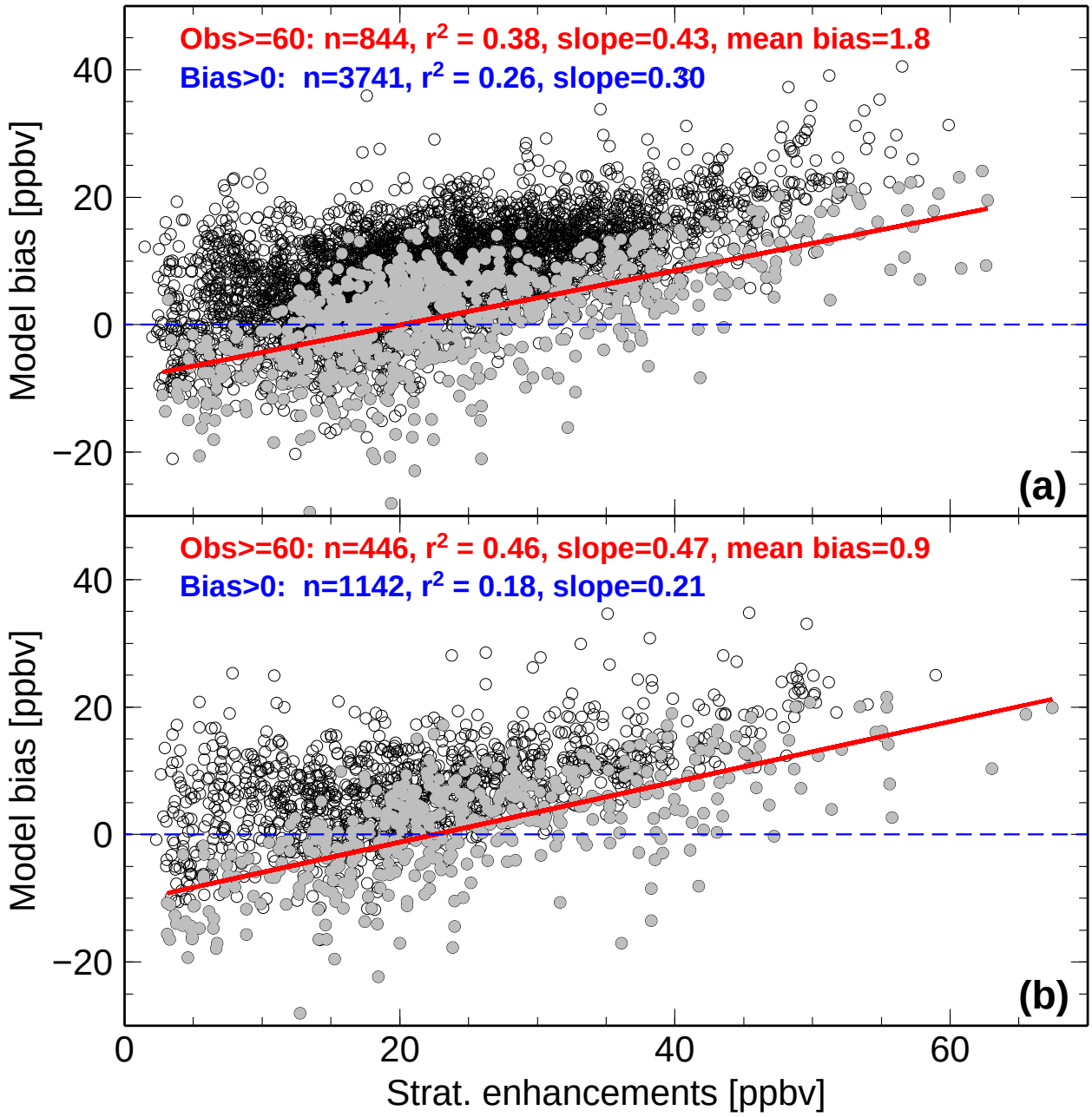


Figure 12. Scatter plots of model biases in surface MDA8 $O_3$ versus stratospheric enhancements for April-June 2010 (a) for AQS sites in EPA Region 8 (red box in Fig.1) and (b) for 15 high-elevation sites (green symbols in Fig.1). Statistics from the linear regression are given for points with observed MDA8 $O_3 \geq 60$ ppb (gray) and points with high model bias (above the blue line).

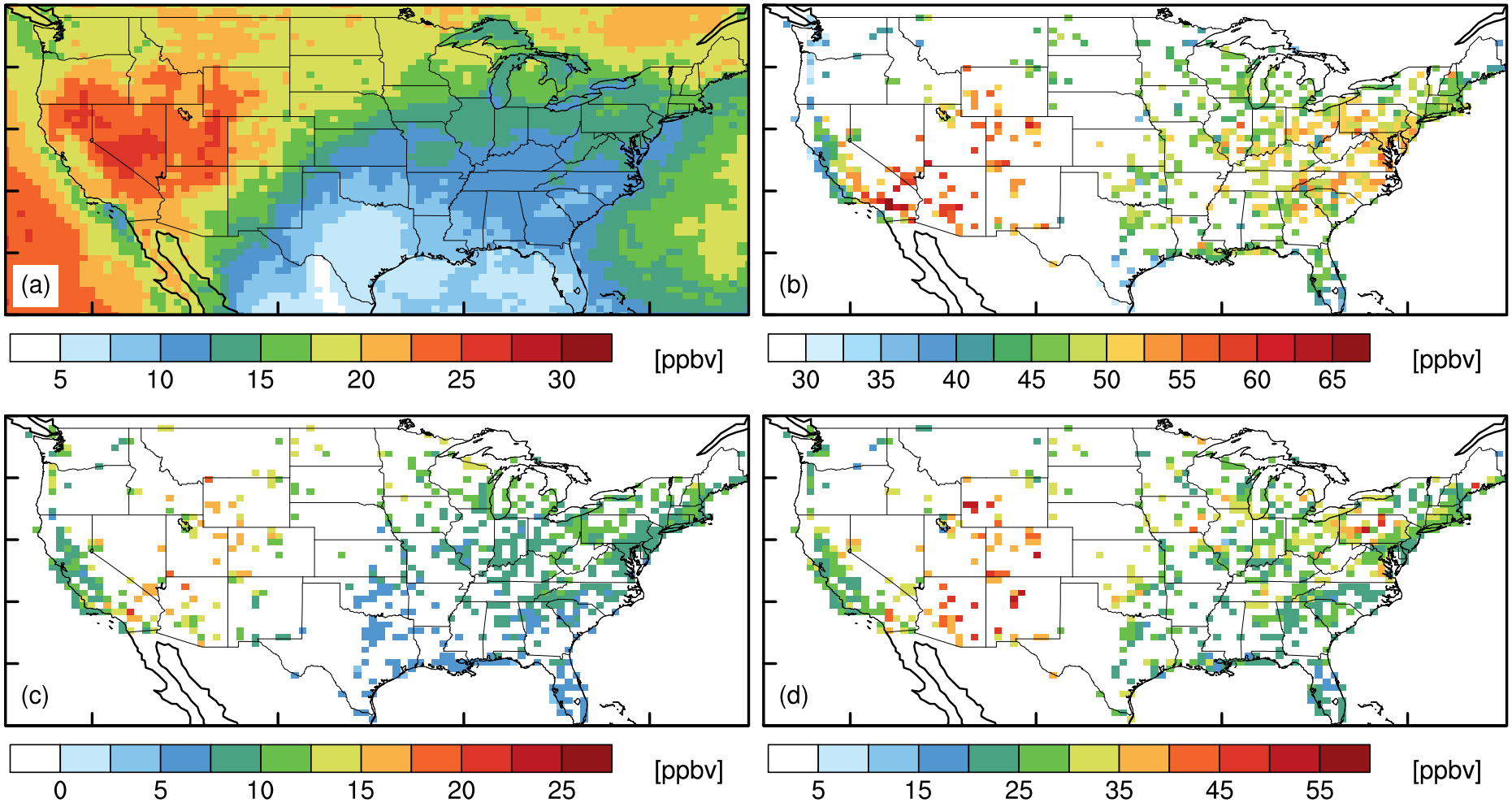


Figure 13. Continental U.S. distributions of (a) median stratospheric contribution to MDA8 surface ozone from April-June 2010 as estimated by the GFDL AM3 model, (b) median MDA8 surface ozone from AQS observations averaged over a 0.625x0.5° grid, (c-d) bias-corrected estimates of the median and maximum stratospheric contribution (Section 4.2). Note the different color scale used to highlight regional variability.

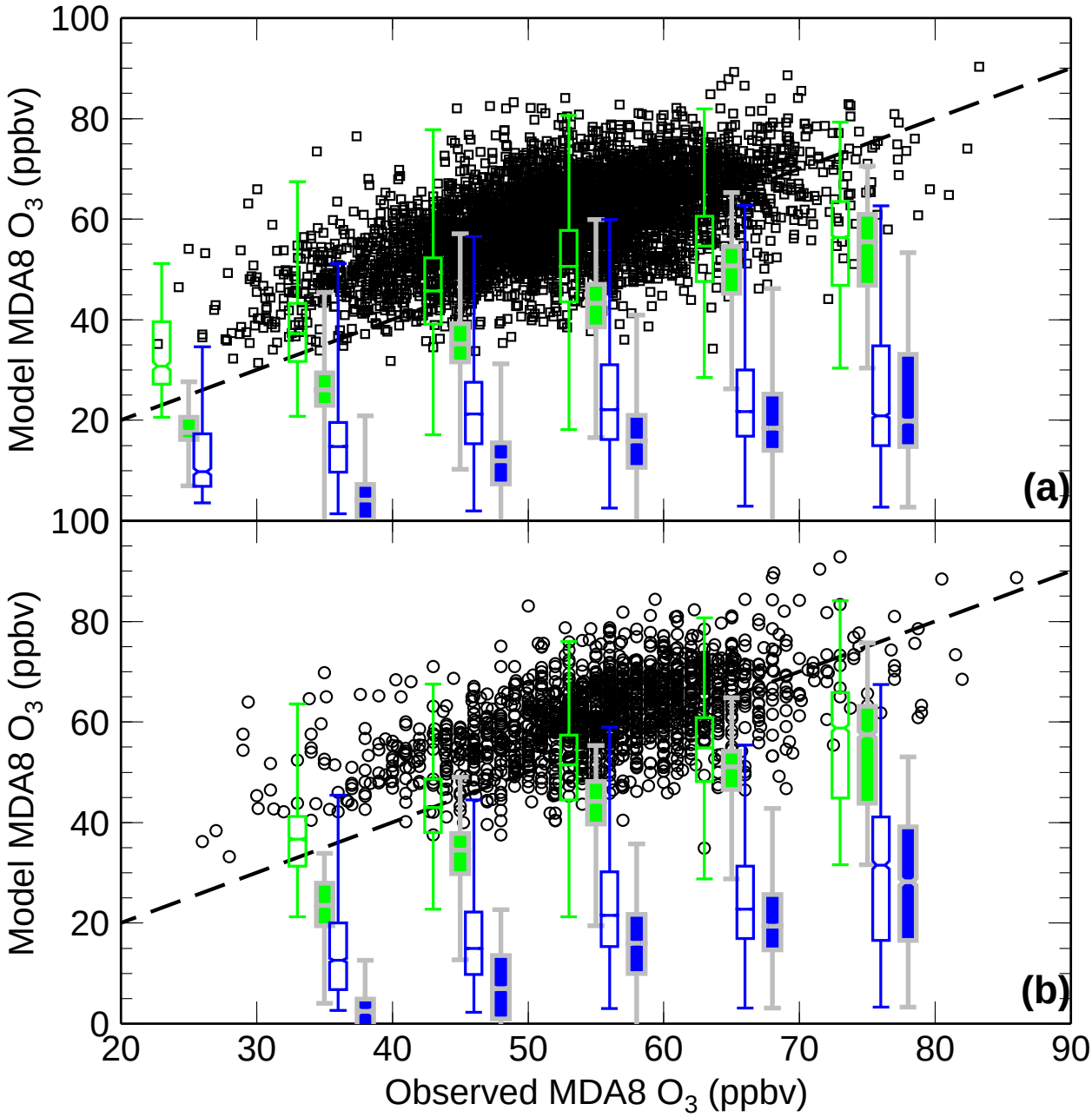


Figure 14. Model versus observed MDA8 surface $O_3$ for April-June 2010 at (a) AQS sites in EPA Region 8 and (b) 15 high-elevation sites (Figure 1). Also shown is the 1:1 line. The box-and-whisker plots (minimum, 25th, 50th, 75th percentiles, and maximum) give statistics of the NA background (green) and the stratospheric contribution (blue) for every 10-ppb bin of observed values. Points greater than 80 ppbv are merged to the 70-80 ppbv range. The filled boxes represent the bias-corrected estimates by assuming that model overestimates of total $O_3$ are entirely driven by excessive stratospheric influence (Section 4.2).